

Assessment of equivalent black carbon variations and its source apportionment over Varanasi, Indo-Gangetic Basin

Prashant Kumar Chauhan^a, Shani Tiwari^{b,c,*}, Dileep Kumar Gupta^a, Akhilesh Kumar^d, Vineet Pratap^a, Abhay Kumar Singh^{a,e,*}

^a Department of Physics, Institute of Science, Banaras Hindu University, Varanasi, 221005, India

^b Aerosol and Cloud Research Lab, CSIR - National Institute of Oceanography, Dona Paula, Goa, 403004, India

^c Academy of Scientific and Innovative Research (AcSIR), Ghaziabad, India

^d Kashi Naresh Government Post Graduate College Gyanpur, Bhadohi, 221304, India

^e DST-Mahamana Centre of Excellence in Climate Change Research, Banaras Hindu University, Varanasi, India



ARTICLE INFO

Keywords:

Black carbon (BC)
Biomass burning
Fossil fuel
Fire counts
Indo-Gangetic Basin
Long range transport

ABSTRACT

In this study, the temporal variation of Equivalent Black Carbon (eBC) and its source apportionment is studied using a yearlong (Dec. 2020–Nov. 2021) multiwavelength Aethalometer (AE-33 model) measurements over Varanasi, located in the central Indo-Gangetic Basin (IGB). Results suggest that mean mass concentrations of eBC vary in the range between 0.46 ± 0.13 to $11.22 \pm 5.09 \mu\text{g m}^{-3}$ with an annual mean value of $\sim 3.57 \pm 2.39 \mu\text{g m}^{-3}$ during the study period. A strong temporal variation in eBC and its components i.e., eBC_{ff} (eBC from fossil fuel), and eBC_{bb} (eBC from biomass burning) are found which shows a large variation on different temporal scales with an average value during winter ($6.21 \pm 3.56 \mu\text{g m}^{-3}$), summer ($5.09 \pm 3.61 \mu\text{g m}^{-3}$), monsoon season ($1.52 \pm 1.03 \mu\text{g m}^{-3}$), and post-monsoon ($3.75 \pm 2.68 \mu\text{g m}^{-3}$). The diurnal variation of eBC shows two different maxima between 07:00–08:00 a.m. and 08:00–10:00 p.m. An inverse relationship between eBC concentration and all meteorological parameters (temperature, wind speed, and boundary layer height) is found except relative humidity. The concentration of eBC increases with respect to RH (up to 70 %) suggesting hygroscopic growth while for higher RH (>70 %) value, eBC concentration decreases and indicates the possible wet scavenging processes in the atmosphere. Source apportionment of eBC using the “Aethalometer Model” reveals that eBC_{ff} is dominant over eBC_{bb} in total eBC loading during the study period. Cluster analysis of HYSPLIT (Hybrid Single Particle Lagrangian Integrated Trajectory) model computed five days airmass back-trajectory suggests that airmass reached at Varanasi passes through a highly dense fire count region over the north-western IGB and surrounding which could be the most responsible for the black carbon loading over the study region.

1. Introduction

Black carbon, a short-lived climate pollutant is a key component of particulate matter (mainly fine particles having a diameter less than $2.5 \mu\text{m}$ i.e., PM_{2.5}) released from the partial combustion of fossil fuels, biomass burning, burning of solid waste, etc. (Bond et al., 2013; Zhang et al., 2021). Due to its relatively finer size, it is easily inhaled and has a detrimental impact on human health (Janssen et al., 2012). Study reported that two major sources of BC i.e., biomass burning and fossil fuel

contribute nearly 80% of the total global BC (Jing et al., 2019). In addition, Klimont et al. (2017) found that transport (~28%) and residential combustion (~58%) are the two major contributors to global BC emissions from fossil fuel while on the regional scale, their contribution to total BC emission changes drastically. Mousavi et al. (2019) also documented that the highest concentration of BC_{ff} occurred during the early morning hours of heavy traffic in Milan city. For BC_{bb}, the concentrations began to rise in the afternoon and reached their highest level at night. This is when wood burning for household heating is at its

Peer review under responsibility of Turkish National Committee for Air Pollution Research and Control.

* Corresponding author. Atmospheric Research Lab. Department of Physics, Institute of Science, Banaras Hindu University, Varanasi-221005, Uttar Pradesh, India.

** Corresponding author. Aerosol and Cloud Research Lab, CSIR - National Institute of Oceanography, Dona Paula, Goa, 403004, India

E-mail addresses: pshani@iitk.ac.in, tiwari@nio.org (S. Tiwari), singhak@bhu.ac.in (A.K. Singh).

highest and the boundary layer heights are at their lowest. BC is highly absorbing in nature (in both visible and infrared spectra) resulting in the second-highest warming agent in the atmosphere (1.1 W m^{-2}) after CO_2 (1.82 W m^{-2}) (Ramanathan and Carmichael, 2008). It has also the potential to modulate the cloud microphysics and precipitation patterns via aerosol indirect and semi-direct effects (IPCC, 2013). BC has an atmospheric lifetime from a few days to weeks resulting in the possibility of being transported over a large distance from one region to another region before being deposited (via wet or dry deposition) (Ding et al., 2023; Tiwari et al., 2020). During the long-range transportation process, the physico-chemical characteristics of BC change via various chemical reactions like photo-oxidation etc. resulting in perturbation in its light absorption characteristics (Srivastava and Ramachandran, 2013; Wang et al., 2016). Light absorption properties of BC largely depend on its emission sources like fossil fuel and biomass burning (Zhang et al., 2021) and are one of the largest uncertainties in global radiative forcing. Hansen et al. (2005) found that soot emitted from fossil fuel burning causes a positive forcing, while soot produced by the combustion of biomass creates a negative forcing. Thus, to control the BC emission and its adverse impacts on climate, human health, and air quality, a better understanding of BC characteristics and accurate estimation of BC emission sources, their relative contribution is very crucial and to be studied on an urgent basis for the development and implementation of mitigation strategies, particularly on the regional scale.

Indo-Gangetic Basin (IGB) is one of the largest populated and polluted river basins in the world and experiences higher aerosol loading (including BC) throughout the year which is associated with strong intra-seasonal to inter-annual variation (Bibi et al., 2017; Lodhi et al., 2013; Rana et al., 2020, 2023; Tiwari et al., 2018 and reference therein). The northwestern part of IGB (Punjab, Haryana, and eastern Uttar Pradesh) experienced large-scale agricultural fires during post-monsoon (paddy residue) and summer (wheat residue) which caused a huge burden of carbonaceous aerosols into the atmosphere (Bansal et al., 2019; Dumka et al., 2018; Rana et al., 2023; Ravindra et al., 2019 and reference therein). These carbonaceous aerosols are transported to the entire southeastern IGB (up to the Bay of Bengal) by prevailing winds (Kant et al., 2022; Kumar et al., 2015; Rana et al., 2023; Tiwari et al., 2016; Vaishya et al., 2016 and reference therein). In detail, Vaishya et al. (2016) found that BC concentration varies between 1 and $51 \mu\text{g m}^{-3}$ over Gorakhpur city with an average value highest during winter ($19 \pm 14 \mu\text{g m}^{-3}$) followed by post-monsoon months ($10 \pm 8 \mu\text{g m}^{-3}$). In another study, Rana et al. (2020) reported a BC concentration of $\sim 1.7\text{--}25.3 \mu\text{g m}^{-3}$ with an average value in the post-monsoon season ($12.1 \pm 5.7 \mu\text{g m}^{-3}$) in the metropolitan city of Kolkata. Kiran et al. (2018) conducted a study on the long-term patterns of BC aerosol at Gadanki and found an annual BC concentration of $\sim 2.2 \mu\text{g m}^{-3}$, with the highest value in March. On the other hand, Dhanbad experiences a strong intra-seasonal variation in BC concentration ranging between 0.84 and $17.0 \mu\text{g m}^{-3}$ with an average value in winter ($8.2 \pm 2.8 \mu\text{g m}^{-3}$), followed by post-monsoon ($6.4 \pm 2.6 \mu\text{g m}^{-3}$) (Singh et al., 2015). High BC loading over Varanasi is also reported from 2009 to 2013 with the value of $11.8 \pm 8.6 \mu\text{g m}^{-3}$ (5-year composite mean) following a similar seasonal pattern i.e., highest in winter months ($21.5 \pm 9.9 \mu\text{g m}^{-3}$) followed by post-monsoon ($17.4 \pm 10.2 \mu\text{g m}^{-3}$) (Srivastava et al., 2019). Interestingly, a large diurnal and seasonal variation in BC is also reported over the Pantnagar (in IGB and near the Himalayan foothill) with an annual mean concentration of $5.5 \pm 4.7 \mu\text{g m}^{-3}$ which is largely associated with meteorological processes and regional/local anthropogenic activities (Joshi et al., 2016).

Several methods are used for source apportionment of BC like (i) carbon isotope (^{14}C) method (Gustafsson et al., 2009), Aethalometer model (Sandradewi et al., 2008a) (ii) macro tracer method (Viana et al., 2013), (iii) chemical mass balance model (Favez et al., 2010), etc. which have merits and demerits on each other. For example, the carbon isotope method can directly quantify the biomass burning and fossil fuel fraction but is limited in time resolution (Chen et al., 2013) while the

Aethalometer model can identify the different BC sources through the multiwavelength absorption coefficient data of BC and thus, widely used worldwide (Sandradewi et al., 2008b). The "Aethalometer model" is an optical method based on the principle of difference in spectral light absorption between complete and incomplete combustion and is used here to estimate the contribution of fossil fuel and biomass burning emission in total BC loading over Varanasi. Although, the study of BC mass concentration and their source apportionment over the Indian region have been carried out by many researchers (Rajesh et al., 2021; Rana et al., 2020; Singh et al., 2015; Tiwari et al., 2016; Vaishya et al., 2016 and reference therein) as discussed in Table 1 yet still a large uncertainty is found which could be due to their emission sources, intensity, and regional meteorological conditions. Thus, an in-depth understanding of BC characteristics on different time scales like diurnal, monthly as well as seasonal scales, source apportionment, and relative contribution is urgently needed, particularly on a regional level (like Varanasi) which will be helpful for different mitigation policies related to air pollution and anthropogenic emissions and National Carbonaceous Aerosol Programme (NCAP) of the government of India. An accurate estimation of BC source apportionment and its relative emission strength will be useful in the global atmospheric chemistry model to reduce climate uncertainties. This study aimed to understand the temporal variation (diurnal, daily, monthly, seasonal) of BC characteristics and their fraction to the total BC mass concentration and the role of long-range transportation in BC loading. In this study, real-time Aethalometer (AE-33 model) data is used for one year i.e. December 2020 to November 2021 and further details about the dataset and others are discussed in upcoming sections.

2. Site description and meteorological conditions

The current study has been carried out at the Department of Physics, Banaras Hindu University, Varanasi ($25.27^\circ \text{N}, 82.98^\circ \text{E}, 80 \text{ m AMSL}$). Varanasi located on the bank of river Ganga in central IGB covers an area of around 112 km^2 , is a holy and densely populated city (2399 residents per square kilometer: Census of India, 2011) surrounded by several small/medium scale industries resulting in relatively higher aerosol loading throughout the year (Tiwari et al., 2018). Varanasi lies in a socio-economic category characterized by low income, where the tertiary sector accounts for the majority (62 %) of the economy. The primary sources of air pollution in this area include particulate matter from road dust, emissions from household cooking, lighting, and heating, as well as the combustion of open waste. The total number of registered motor vehicles in Varanasi is seven lakhs seventy-seven thousand one hundred thirty which plays a major role in the contribution of fossil fuel burning emissions (Dasgupta and Srikanth, 2020). Being in central IGB, Varanasi experiences four seasons such as winter (December-January-February), summer (March-April-May), monsoon (June-July-August-September), and post-monsoon (October-November) resulting in large heterogeneity in aerosol loading and seasonal variation due to different emission sources and meteorological conditions (Srivastava et al., 2019). For example, during the summer season higher aerosol loading is mostly dominated by coarse-mode aerosol through the long-range transportation of dust from nearby arid regions (Tiwari et al., 2018). During the winter season, under suitable meteorological conditions, these aerosols cause dense fog which leads to a reduction in atmospheric visibility. In addition, during the monsoon season, Varanasi also experiences marine aerosols (Tiwari and Singh, 2013) and an intense rainfall of about 71% in the monsoon season (Murari et al., 2017). Meteorological factors like air temperature (temp), relative humidity (RH), wind speed (WS), and wind direction (WD) data were taken from the Central Pollution Control Board (CPCB) installed at Araldi Bazar, Varanasi at 5 km from the measuring site in BHU, Varanasi. Meteorological data received by this CPCB location is representative of the measurement site in Fig. 1. The data is freely available and quality checks are performed by CPCB. Boundary layer height (BLH) data were

Table 1

Comparison of eBC at different locations in India.

S. No	Locations	Period	eBC Concentrations ($\mu\text{g m}^{-3}$)	References
1	BHU, Varanasi (25.27° N; 82.98° E; 80 m) (VNS)	December 2020–November 2021	3.57 ± 2.39	Present Study
2	IITD, New Delhi (28.53° N; 77.18° E; 209 m) (IITD)	August 2020–November 2020	12.6 ± 8.2	Goel et al. (2021)
3	Agra (27.10° N; 78.02° E; 170 m) (AGRA)	March–May 2019	6.9	Gupta et al. (2023)
		March–May 2020	3.9	
4	NPL, New Delhi (28.63° N; 77.17° E; 216 m) (NPLD)	September 2019–August 2020	5.02 ± 4.40	Malik et al. (2022)
5	IMD, New Delhi (28.59° N; 77.22° E; 253 m) (IMDD)	2016–2018	13.57 ± 8.4	Kumar et al. (2020)
6	Panchgaon village, Gurugram (28.2° N; 76.5° E; 266 m) (PVG)	April 2015–March 2016	7.2 ± 0.3	Dumka et al. (2018)
7	Varanasi (25.27° N; 82.98° E; 80 m) (VNS)	1 st January 2009–31 st December 2016	9.7 ± 6.3	Singh et al. (2021)
8	Patiala (30.33° N; 76.40° E; 257 m) (PTL)	January 2009–December 2011	8.43 ± 3.14	Shaik et al. (2019)
	Dehradun (30.34° N; 78.04° E; 640 m) (DDUN)	January 2011–December 2017	3.36 ± 1.26	
9	IITK, Kanpur (26.46° N; 80.32° E; 127 m) (IITK)	September 2007–July 2011	7.96	Kanawade et al. (2014)
10	Karachi (24.85° N; 67.03° E; 10 m) (KRC)	March 2006–December 2008	5.5 ± 2.7	Bibi et al. (2017)
11	Manora Peak, Nainital (29.4° N; 79.5° E; 1951 m) (MPNL)	November 2004–December 2007	0.99 ± 0.02	Dumka et al. (2010)
12	Jamshedpur (23.33° N; 86.33° E; 150 m) (JSD)	September–November 2021	18.22	Hussain et al. (2023)
	Dhanbad (23.78° N; 86.5° E; 222 m) (DNB)		14.18	
	Ranchi (23.37° N; 85.33° E; 651 m) (RNC)		10.39	
13	Ooty (11.42° N; 76.72° E; 2240 m) (OOTY)	January–February 2021	0.89 ± 0.26	Sivasankaran et al. (2022)
		March 2021	1.46 ± 0.62	
14	Chennai (12.99° N; 80.23° E; 6.7 m) (CHN)	21 st January–23 rd March 2020	4.88 ± 1.94	Vaishya et al. (2023)
		24 th March–30 th June 2020	1.69 ± 0.69	
15	Jamshedpur city (23.33° N; 86.33° E; 150 m) (JSD)	(3 rd January–23 rd March) & (1 st April–June 14 2020)	11.71 ± 3.33	Ambade et al. (2021)
			2.46 ± 0.95	
16	IIT Guwahati (26.1878° N; 91.6916° E; 49 m) (IITG)	12 th February–3 rd July 2020	5.75 ± 4.24	Singh and Gokhale (2022)
17	Ahmedabad (23.03° N; 72.55° E; 53 m) (ABD)	25 th March–31 st May	2.2 ± 0.7	Rajesh and Ramachandran (2022)
		1 st June–31 st December 2020	4.3 ± 2.3	Rajesh et al. (2021)
18	Ahmedabad (23.03° N; 72.55° E; 53 m) (ABD)	January–December 2019	6.6 ± 4.1	
	Anand (22.55° N; 72.93° E; 39 m) (AND)		4.9 ± 2.9	
19	IITM Pune (18.54° N; 73.80° E; 571 m) (IITM)	April 2018–February 2019	3.9 ± 2.8	Meena et al. (2021)
	Mahabaleshwar (17.92° N; 73.65° E; 1348 m) (MBL)		1.4 ± 0.9	
20	Mohanpur (22.95° N; 88.52° E; 17 m) (MHP)	May 2018–February 2020	7.76 ± 4.67	Rana et al. (2023)

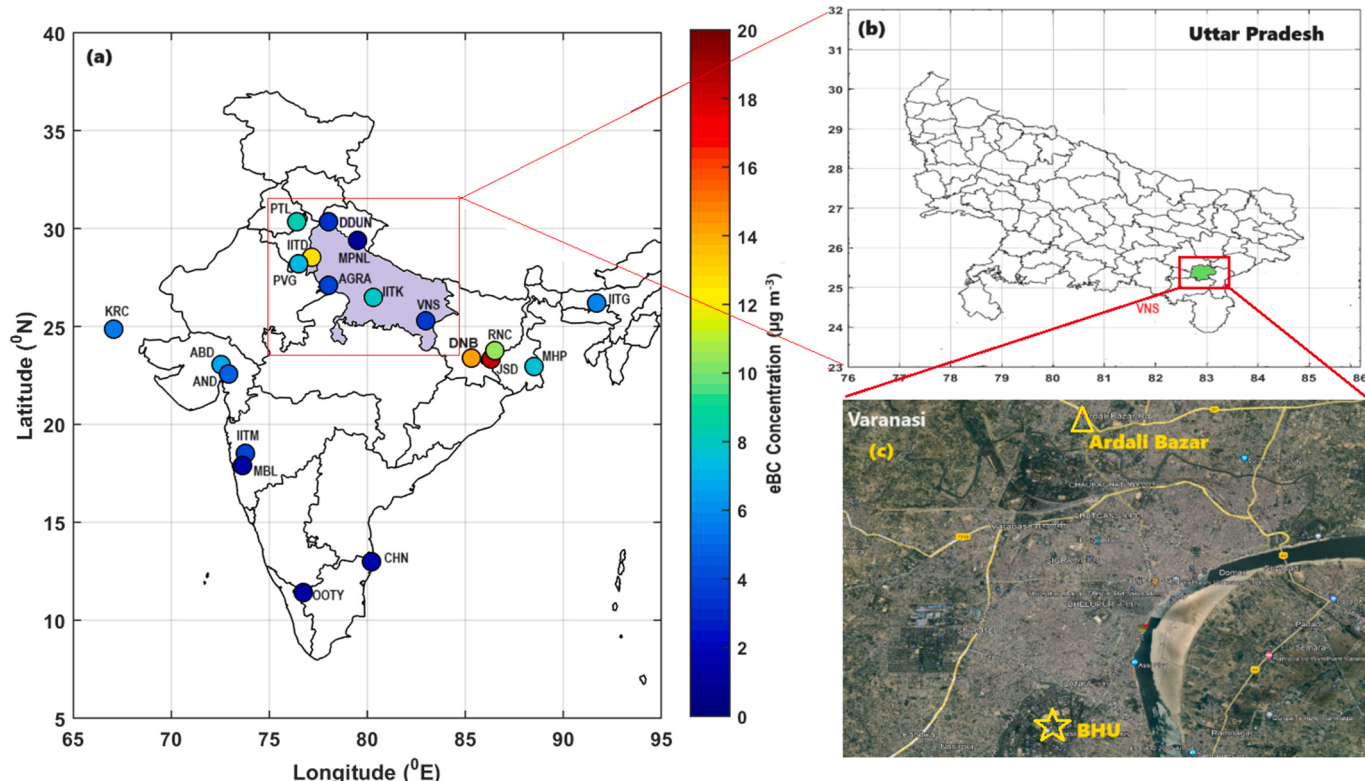


Fig. 1. Location of observational site Varanasi (25.27° N; 82.98° E) in Central IGB region, India. The image in a square box is the Google map of the Varanasi. The CPCB site from where the measurements are being made is also pinned on the map. Different color circles show the BC values reported from different locations given in Table 1.

downloaded from ERA5 over the measuring location. Fig. 2 portrays the changes in monthly averages of climatic parameters, encompassing relative humidity (RH), temperature (temp), boundary layer height (BLH), wind speed (WS), and wind direction (WD). During the study period, the yearly mean temperature was approximately 27.09 ± 6.14 °C. Notably, January had an average temperature of around 15 °C, rendering it the coldest month in comparison to others. Conversely, April exhibited elevated temperatures, reaching about 34 °C due to its position within the summer season. The temperature followed an ascending pattern from January to April, succeeded by a subsequent decline from April to November. The average annual relative humidity (RH) was measured at roughly $66 \pm 12\%$, fluctuating between 39% in April and 76% in September. Similarly, the BLH exhibited a resemblance same as temperature fluctuations, ranging from approximately 0.268 km in December to 0.794 km in April. On the other hand, May witnessed the highest wind speed (1.8 m/s), while November encountered the lowest wind speed (0.6 m/s), culminating in an annual average of 1.03 ± 0.35 m/s. Consistently, the prevailing wind direction throughout the year at the study site was south and south-westerly. Given the variation in emission sources and atmospheric transport paths, acquiring comprehensive meteorological data becomes imperative for assessing the influence of ambient aerosols on the atmospheric radiation budget.

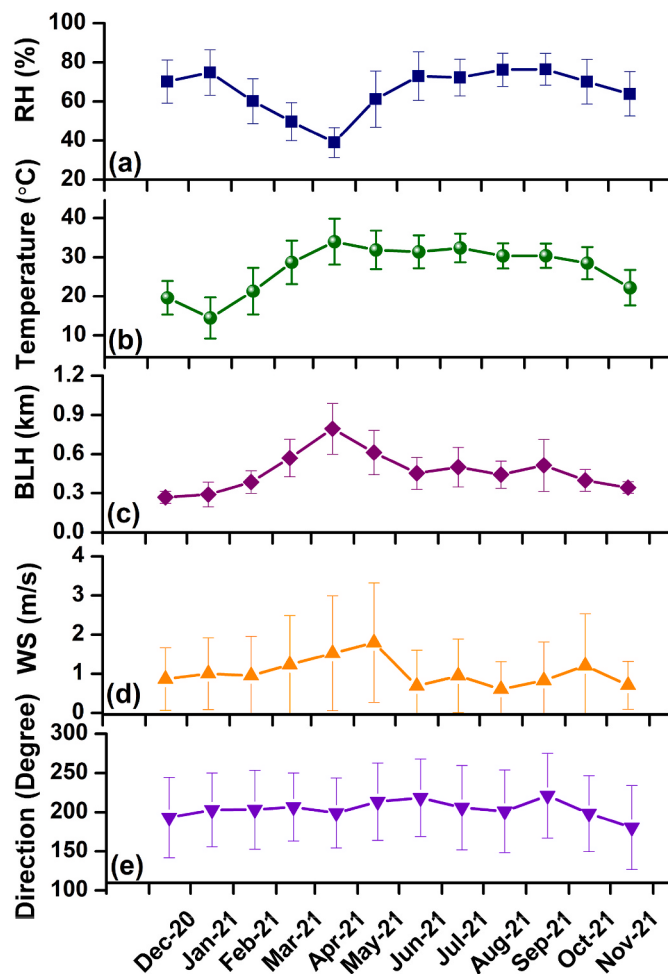


Fig. 2. Monthly mean variation of (a) relative humidity (%), (b) temperature (°C), (c) BLH (km) (d) wind speed (m/s), and (e) wind direction (degree) during the study period over Varanasi. Here vertical lines represent the standard deviation from the mean.

3. Measurement and methodology

3.1. BC measurement and source apportionment

Black Carbon mass concentration was measured at every minute using an Aethalometer (AE-33 Magee scientific) having a flow rate of 2 L min^{-1} . This instrument is based on the Beer-Lambert law and employs dual-spot technology. It is operated in a room situated on the top floor of the Department of Physics building and room temperature is carefully monitored and maintained. The instrument's intake duct is perched at a height of 3 m above the building's rooftop, which sits at a total height of 10 m above the ground. It measures an attenuated beam of light at seven different wavelengths (i.e., 370, 470, 520, 590, 660, 880, and 950 nm) from ultraviolet to near-infrared spectrum through filter tape on which BC particles are deposited and measured. Aethalometer AE-33 multi-wavelength measurements can be used to calculate the source apportionment of BC from different sources like fossil fuel combustion and biomass burning (Ziola et al., 2021). Biomass-burning sources that are a major contributor to the organic aerosols present in the BC, exhibit more UV absorption than near-infrared absorption. BC is the main constituent of emissions from fossil fuels, and it exhibits high absorption at the 880 nm (near IR-region) wavelength (Goel et al., 2021).

The Aethalometer measures the optical attenuation of light using seven specific wavelengths: 370 nm, 470 nm, 520 nm, 570 nm, 660 nm, 880 nm, and 950 nm. Nevertheless, the concentration of BC is evaluated specifically at a wavelength of 880 nm. Mineral dust, which is a significant component of light-absorbing aerosols, exhibits intense absorption in the blue and green portions of the visible spectrum while showing minimal absorption in the red portion. At a wavelength of 880 nm, aerosol species such as organic carbon and mineral dust show minimal absorption, indicating that the absorption can be solely attributed to BC. For data obtained by using optical absorption methods, it is recommended to utilize equivalent black carbon (eBC) instead of black carbon, and an appropriate mass absorption cross-section (MAC) should be used for the transformation of the light absorption coefficient into the mass concentration measurement (Petzold et al., 2013). The manufacturer provides mass absorption cross-section values of 18.47, 14.54, 13.14, 11.58, 10.35, 7.77, and $7.19 \text{ m}^2 \text{ g}^{-1}$ at wavelengths of 370, 470, 520, 590, 660, 880, and 950 nm, respectively are used (Rathod and Sahu, 2022; Weingartner et al., 2003). The relationship between the absorption coefficient (b_{abs}) and the mass absorption cross-section (MAC) is expressed as follows:

$$b_{abs}(\lambda) = BC(\lambda) * MAC(\lambda) \quad (1)$$

The Aethalometer model was developed primarily to estimate the contribution of fossil fuels (eBC_{ff}) and biomass (eBC_{bb}) to total eBC loading. This model assumes that the absorption coefficient is proportional to the combination of percentages of fossil fuels and biomass burned (Herich et al., 2011):

$$b_{abs}(\lambda) = b_{abs}(\lambda, ff) + b_{abs}(\lambda, bb) \quad (2)$$

where $b_{abs}(\lambda, ff)$ and $b_{abs}(\lambda, bb)$ are aerosol absorption coefficients for burning fossil fuels and burning biomass at a given wavelength λ . Following Angstrom power law, the absorption exponent (α) for burning pure fossil fuels and biomass can be given as:

$$\frac{b_{abs}(\lambda_1, ff)}{b_{abs}(\lambda_2, ff)} = \left(\frac{\lambda_1}{\lambda_2} \right)^{-\alpha_{ff}} \quad (3)$$

$$\frac{b_{abs}(\lambda_1, bb)}{b_{abs}(\lambda_2, bb)} = \left(\frac{\lambda_1}{\lambda_2} \right)^{-\alpha_{bb}} \quad (4)$$

where α_{ff} and α_{bb} are the absorption exponents of concerning wavelengths λ_1 (470 nm) and λ_2 (880 nm) respectively (Sandradewi et al., 2008a).

It is possible to calculate eBC_{ff} with the help of the following

equations.

$$eBC_{ff} = eBC \frac{b_{abs}(\lambda_{1,ff})}{b_{abs}(\lambda)} \quad (5)$$

$$eBC = eBC_{ff} + eBC_{bb} \quad (6)$$

$$eBC_{bb} = eBC - eBC_{ff} \quad (7)$$

In this study, α_{ff} and α_{bb} values employed for apportionment are 1 and 2, respectively. The 'Aethalometer model' used to calculate the proportion of biomass burning is sensitive to α_{bb} values and therefore determining its value depends on the specific location and sources. In the current scenario, the aerosol source region extends across a broad geographic area, and the aerosols undergo extensive mixing and aging before reaching the monitoring station, therefore, the average value of α_{bb} is set to 2. Earlier studies have used the same values of Angstrom exponent over the IGB region (Kumar et al., 2020; Tiwari et al., 2015; Vaishya et al., 2016).

3.2. MODIS fire count and HYSPLIT air mass back trajectory model

To investigate the large-scale open biomass burning and its association with BC loading, the MODIS (Moderate Resolution Imaging Spectroradiometer) active Fire Counts products over the Indian region for the study period are used. MODIS is a sensor board on NASA's Terra and Aqua satellite having a swath of 2330 km, provides earth and atmospheric radiance across 36 wide spectral bands ranging between 0.41 and 15 μm , with spatial resolution varying from 250 m to 1 km. The active fire count data products (MCD14) are processed through the MODAPS (MODIS Adaptive Processing System) using the enhanced contextual fire detection algorithm (Giglio et al., 2003) and can be freely downloaded from the FIRMS (Fire Information for Resource Management System: https://firms.modaps.eosdis.nasa.gov/active_fire/). Further details about the fire detection algorithm and related errors are discussed elsewhere (Giglio et al., 2003; Justice et al., 2002). Earlier researchers have used active fire count data as a proxy for ground forest fire assessment and analysis of crop residue burning occurrences worldwide (Babu et al., 2016; Chowdhury and Hassan, 2015; Hong et al., 2023; Jethva, 2022; Vadrevu et al., 2011; Vadrevu and Lasko, 2015). Furthermore, in the current study, fires with high-confidence level data (>80 %) were used (Shaik et al., 2019). To decipher possible source regions, their transport routes, and relative contributions within the designated area, five-day air mass back trajectories were computed (1000 m above ground level) at the study site by using National Oceanic and Atmospheric Administration (NOAA) HYSPLIT (Hybrid Single-Particle Lagrangian Integrated Trajectory) model and NCEP (National Center for Environmental Prediction) reanalysis wind dataset as input (Rolph et al., 2017; Stein et al., 2015). These air mass back trajectories provide 4-D information (lat, long., altitude, and time) about the airmasses which will be helpful to establish source receptor relationships. These computed daily airmass back trajectories were further used to perform cluster analysis using the total spatial variance (TSV) method. Further details about the back trajectory and cluster analysis are discussed elsewhere (Taubman et al., 2006; Tiwari et al., 2023).

4. Results and discussions

4.1. Temporal variation of eBC and its components

4.1.1. Monthly variation

The daily mean mass concentration of eBC is shown in Fig. 3 which exhibits a wide range of 0.46 ± 0.13 to $11.22 \pm 5.09 \mu\text{g m}^{-3}$ over the entire period, with an annual mean concentration of $3.57 \pm 2.39 \mu\text{g m}^{-3}$. Due to some technical issue in the aethalometer, data were not

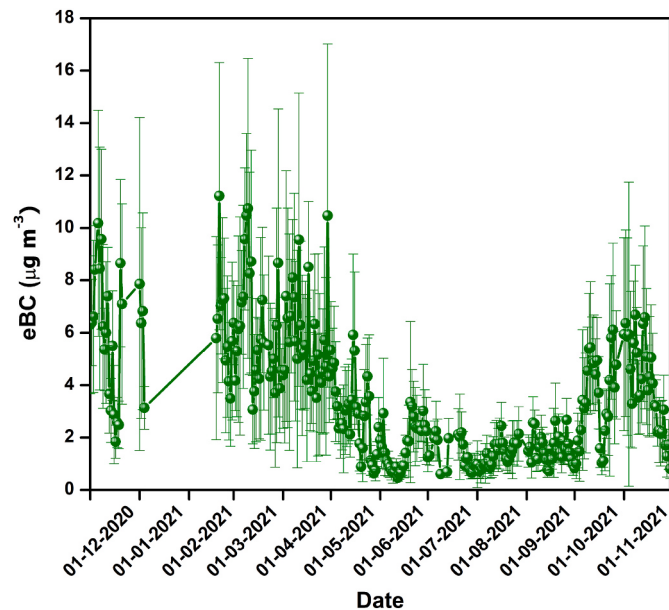


Fig. 3. Daily mean variation of eBC mass concentration ($\mu\text{g m}^{-3}$) over Varanasi during the study period. The vertical lines at each data point represent the standard deviation from their mean value.

acquired from January 05, 2021 to February 17, 2021. The monthly mean value of eBC is given in (Fig. 4) which shows maximum eBC concentration in February ($6.63 \pm 3.61 \mu\text{g m}^{-3}$) while minimum in July ($1.34 \pm 0.82 \mu\text{g m}^{-3}$). Starting in August with an average mass concentration of $1.35 \pm 0.81 \mu\text{g m}^{-3}$, eBC levels were consistently found to be increased ($4.09 \pm 2.81 \mu\text{g m}^{-3}$) in November. The highest mass concentration of eBC was seen during the winter season ($6.21 \pm 3.56 \mu\text{g m}^{-3}$), followed by the summer season ($5.09 \pm 3.61 \mu\text{g m}^{-3}$), and thereafter decreased until the monsoon season ($1.52 \pm 1.03 \mu\text{g m}^{-3}$). Subsequently, it has increased during the post-monsoon season ($3.75 \pm 2.68 \mu\text{g m}^{-3}$). The eBC values in the winter, summer, and post-monsoon months are found to be consistently high, as indicated by the 95th percentile. This suggests that there are episodically higher eBC throughout the months which cause overall higher mean values. In

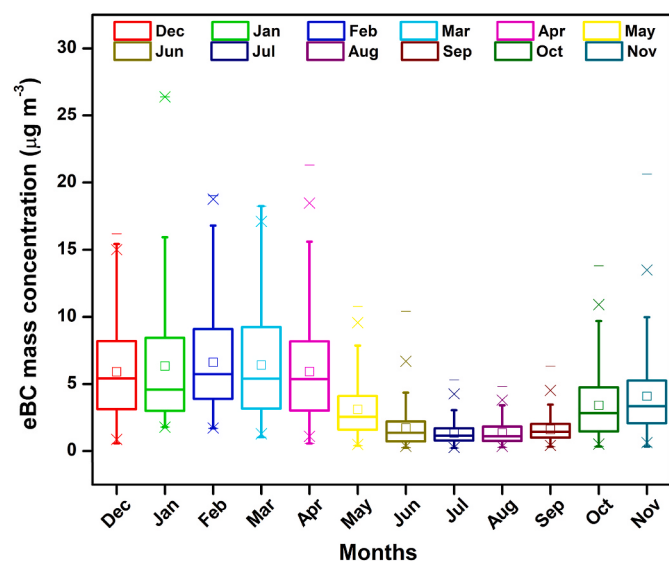


Fig. 4. Box and Whisker plot of the monthly mean variation of eBC concentration ($\mu\text{g m}^{-3}$). The lower and upper box boundaries show 25th and 75th percentiles, solid line and square inside the box are median and mean, whereas lower and upper horizontal caps are 10th and 90th percentiles.

contrast, during the monsoon months, there is a low occurrence of episodes with high eBC mass concentration, as indicated by almost coinciding mean and median eBC and low variation in the 95th percentile which could be due to extensive aerosol scavenging through wet deposition. Thus, such large variations in eBC mass concentration can be attributed to several critical factors, including fluctuations in precipitation levels, variations in synoptic wind patterns, changes in boundary layer height (BLH), and alterations in aerosol source intensity. For example, during summer months higher solar radiation causes higher ambient temperature resulting in a strong convection activity which is a favourable condition for dilution as BLH is increasing. On the other hand, during the winter season, Varanasi has significant emissions of eBC due to widespread household consumption. A dry and stable boundary layer over the region developed an atmospheric condition that inhibits the diffusion and transportation of eBC aerosols and results in the accumulation of eBC pollutants. Recent studies have also reported similar variations in eBC concentration in India with different magnitudes as given in Table (1). Earlier research conducted in Delhi by Kumar et al. (2020) reported eBC concentrations of $13.57 \pm 8.4 \mu\text{g m}^{-3}$ between 2016 and 2018. In contrast, Malik et al. (2022) observed lower eBC levels of $5.02 \pm 4.40 \mu\text{g m}^{-3}$ from September 2019 to August 2020, including the lockdown period. Subsequently, eBC concentrations increased to $12.6 \pm 8.2 \mu\text{g m}^{-3}$ in the period from August 2020 to November 2020, as documented by Goel et al. (2021). The variation in these results can be partially attributed to the impact of the COVID-19

lockdown, during which all forms of human activities and emissions from factories were temporarily absent. Gupta et al. (2023) reported the average monthly mass concentration of eBC at Agra was 4.7, 3.4, and $3.3 \mu\text{g m}^{-3}$ in March, April, and May of 2020, respectively. The reduced eBC concentrations during 2020 could potentially be attributed to the extensive lockdown imposed to mitigate the spread of the COVID-19 pandemic. According to Kaur et al. (2020), the annual mean eBC mass concentration at 880 nm was found to be the highest ($12.56 \pm 5.06 \mu\text{g m}^{-3}$) in 2011 while the lowest ($7.26 \pm 2.76 \mu\text{g m}^{-3}$) in 2015 over Agartala.

4.1.2. Frequency distribution of eBC, eBC_{ff} , and eBC_{bb}

As discussed above, Varanasi experiences a wide range of eBC concentrations which shows a large temporal variation. Thus, to investigate the highest eBC concentration range on a seasonal basis, a frequency distribution histogram was plotted (Fig. 5). The highest point of the curve corresponds to the concentration with the maximum frequency of occurrence. The higher levels of air pollution in northwest India stem from multiple elements. These encompass practices such as agricultural burning, higher emissions due to the combustion of wood, dung cakes, and waste materials for heating, a stable boundary layer height (BLH) that traps pollutants close to the Earth's surface, reduced efficacy of rainfall in cleansing pollutants, and the prevalence of low wind speeds. The distribution of eBC frequencies across the four seasons at the observation site is depicted in Fig. 5a-d. The samples were categorized

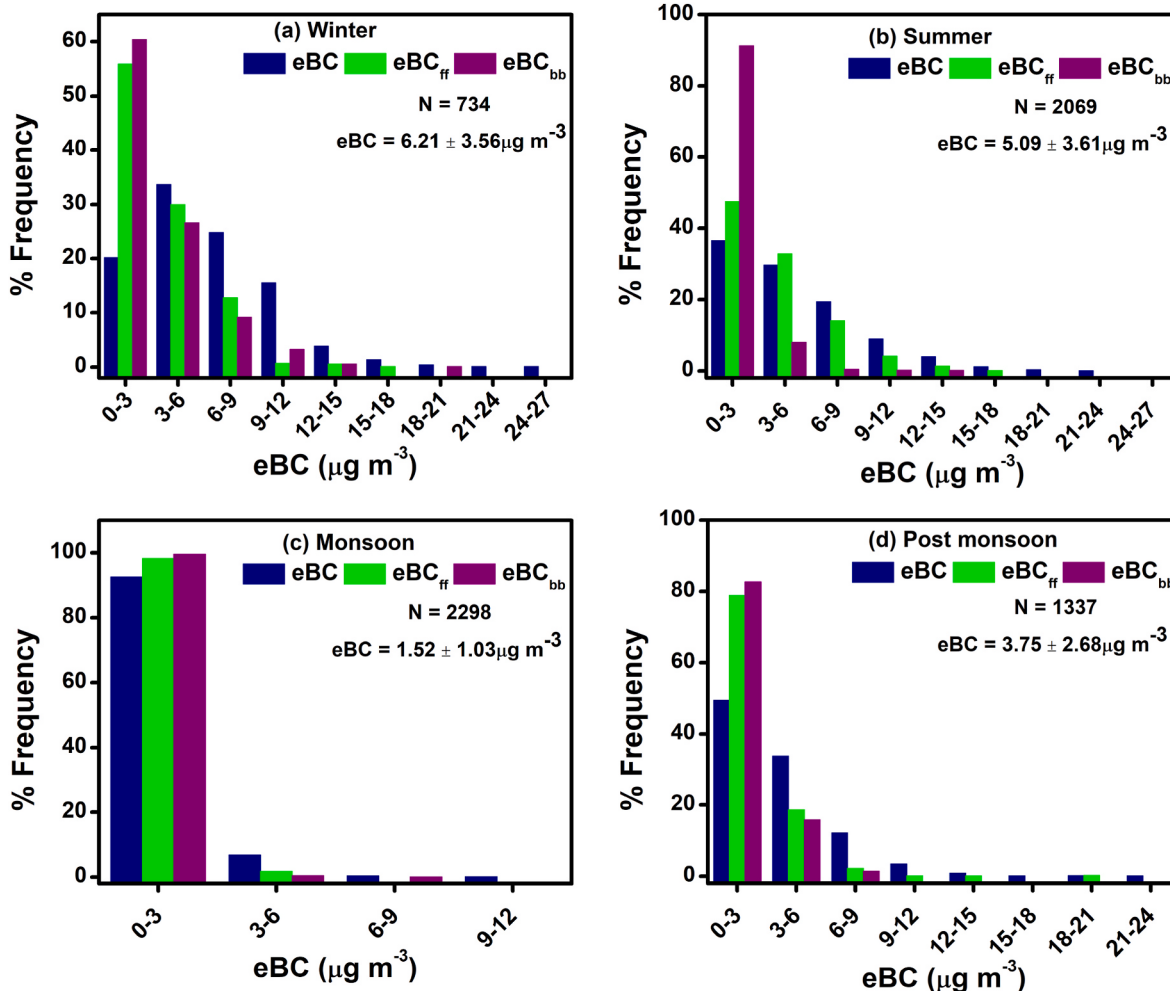


Fig. 5. Frequency distribution of eBC for (a) winter, (b) summer, (c) monsoon, and (d) post-monsoon. The total number of datasets in each season is given by 'N' while the seasonal mean of eBC mass concentration ($\mu\text{g/m}^3$) with $\pm 1\sigma$ is also given within figure.

into nine bin-size groups, ranging from 0 to $27 \mu\text{g m}^{-3}$ with an interval of $3 \mu\text{g m}^{-3}$. The dataset containing hourly eBC mass concentration measurements have been chosen to create a frequency distribution diagram. In the winter season, eBC concentrations predominantly 25% and 38% fell within the $0\text{--}3$ and $3\text{--}6 \mu\text{g m}^{-3}$ range respectively, with only 14% of concentrations observed above $9 \mu\text{g m}^{-3}$. Similarly, during the summer season, eBC concentrations within the $0\text{--}3$ and $3\text{--}6 \mu\text{g m}^{-3}$ range were mostly found to be 39% and 33%, respectively, with only 9% of concentrations surpassing $9 \mu\text{g m}^{-3}$. In the monsoon season, a significant portion (89%) of eBC concentrations were lying within the $0\text{--}3 \mu\text{g m}^{-3}$ range, whereas merely 1% of concentrations were above $6 \mu\text{g m}^{-3}$. Moving to the post-monsoon season, eBC concentrations were mainly (49%) and (37%) in the $0\text{--}3$ and $3\text{--}6 \mu\text{g m}^{-3}$ range respectively, with only 3% of concentrations exceeding $9 \mu\text{g m}^{-3}$.

4.1.3. Monthly and diurnal variation of eBC, eBC_{ff} , and eBC_{bb}

Fig. 6 shows the monthly mean concentrations of eBC, eBC_{ff} , and eBC_{bb} at seven distinct Aethalometer wavelengths. This graphical representation emphasizes the fluctuations in eBC concentrations across varying wavelengths. These variations arise due to the existence of different absorbing aerosol species (combining eBC with light-absorbing OC), each characterized by unique spectral MAC values. The variation in

eBC concentrations at these specific wavelengths allows for insights into both the sources of eBC and the atmospheric conditions affecting its distribution. The highest mean contribution of eBC is observed such as 12.44 ± 9.06 , 9.62 ± 6.97 , 8.45 ± 6.14 , 7.71 ± 5.60 , 6.93 ± 5.04 , 6.63 ± 3.62 , and $6.65 \pm 3.63 \mu\text{g m}^{-3}$ at seven wavelengths 370, 470, 520, 590, 660, 880, and 950 nm respectively. The higher concentration of eBC observed in winter can be ascribed to a range of contributing factors. These factors encompass agricultural burning in northwest India, elevated emissions stemming from the combustion of wood, dung cakes, and waste materials utilized for heating, the confinement of pollutants near the surface due to shallow boundary layer heights (BLH), reduced effectiveness of rainfall in cleansing the atmosphere, and tranquil wind patterns.

The diurnal variations of eBC mass concentrations, as well as their components i.e., eBC_{ff} and eBC_{bb} during different months, are shown in Fig. 7. The concentration of eBC exhibits a persistent and robust diurnal pattern during the study period, characterized by two distinct peaks and troughs. The initial peaks in eBC mass concentration observed between 07:00 and 08:00 are ascribed to the rise in human-induced activities, after which the eBC concentration begins to decline. The higher volume of vehicular traffic contributes to the occurrence of secondary peaks in the concentrations of eBC during the evening hours, specifically between

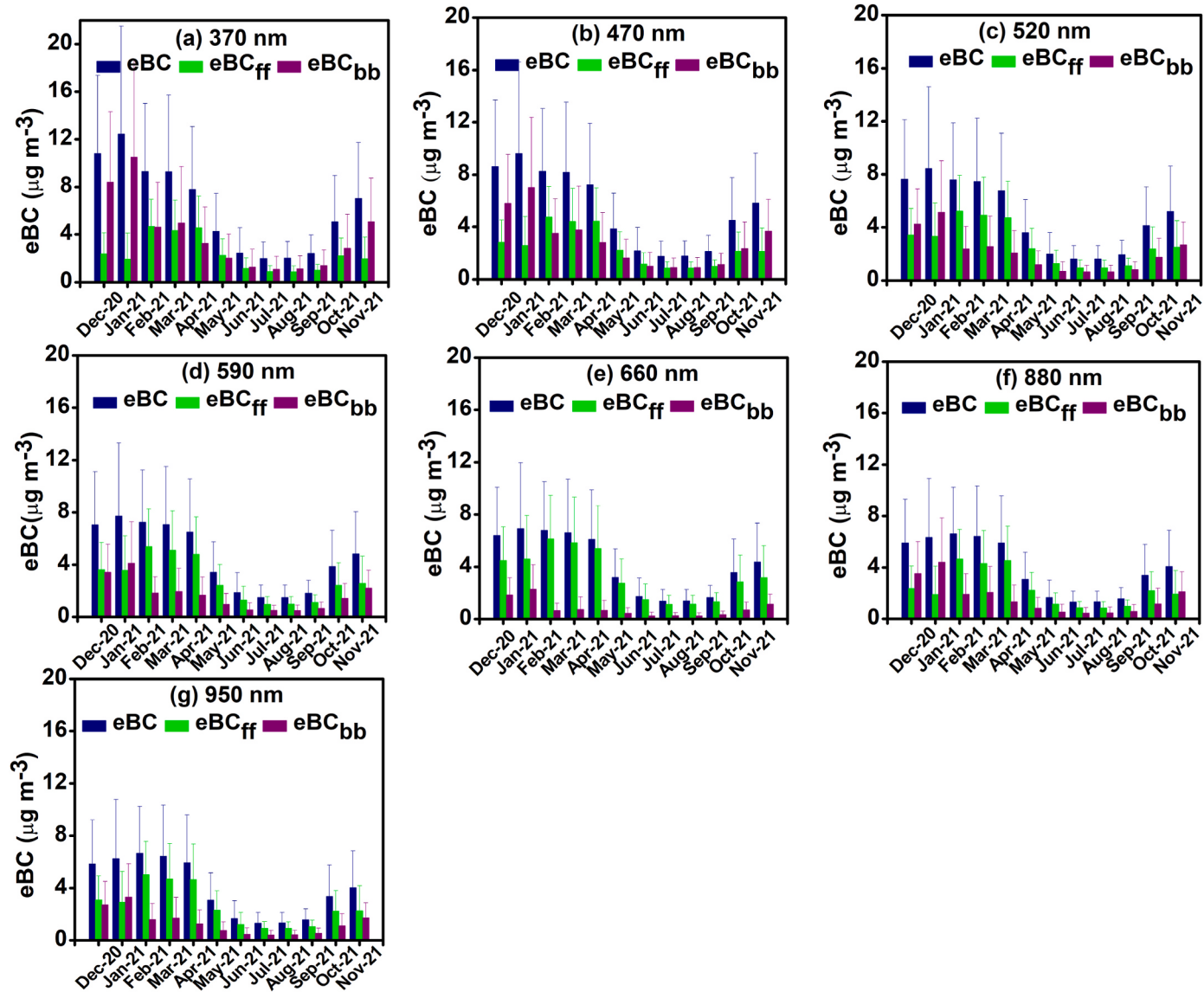


Fig. 6. Monthly mean variation of eBC, eBC_{ff} , and eBC_{bb} at all seven wavelengths over Varanasi.

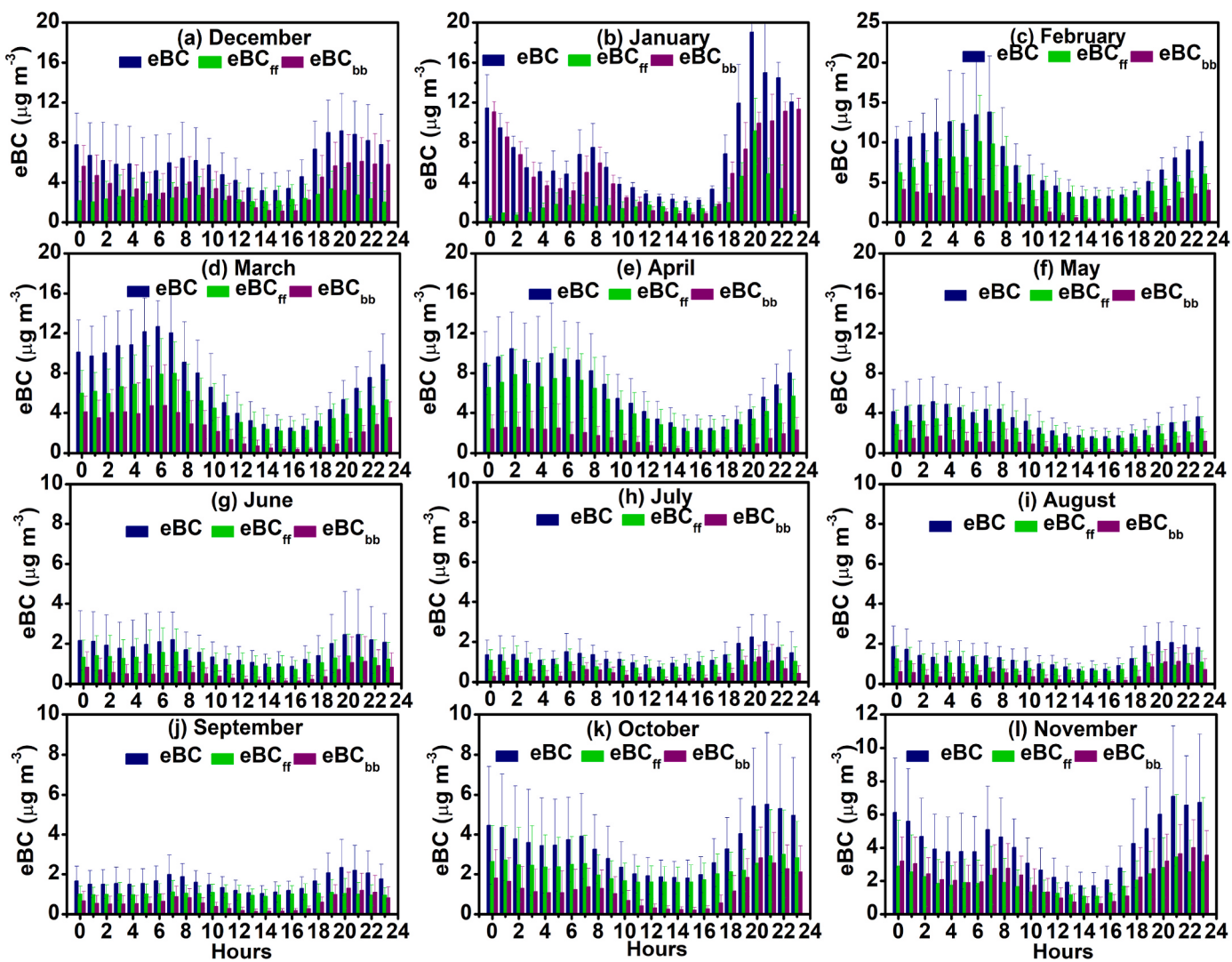


Fig. 7. Month-wise diurnal variation of eBC, eBC_{ff}, and eBC_{bb} mass concentrations over Varanasi.

20:00 and 22:00. The maximum and minimum contribution of eBC are observed during January ($19.05 \pm 10.39 \mu\text{g m}^{-3}$) and August ($0.74 \pm 0.27 \mu\text{g m}^{-3}$) respectively. After this period, there is a substantial reduction in traffic, resulting in a corresponding decrease in the production of eBC aerosols. The eBC aerosols experience atmospheric clearance through gravitational settling, resulting in a decrease in eBC mass concentration during the early morning hours, specifically around 03:00–04:00, except during the summer season. The mass concentrations of eBC are significantly impacted by anthropogenic sources and atmospheric dynamics, namely the boundary layer height (BLH) and wind patterns (Ramachandran et al., 2021). The diurnal contribution of the eBC_{ff} and eBC_{bb} exhibits constant variation throughout the year, characterized by two distinct peaks and troughs. eBC_{ff} is found to be the most significant contributor to eBC levels seen in Varanasi throughout the year except in the winter months. The nocturnal and early morning periods exhibit a higher proportion of fossil fuel combustion (eBC_{ff}) in eBC concentrations and can be attributed to the presence of surface inversion that leads to the accumulation of primary pollutants associated with eBC (Srivastava et al., 2012; Vadrevu et al., 2012). The study revealed that eBC_{bb} made a higher contribution to the levels of eBC throughout the morning and evening periods, especially in winter months, which can be attributed to the rise in emissions from wood burning in both residential and industrial sectors. Likewise, significant variations in eBC concentration have been documented across various

regions in India, such as Varanasi (Srivastava et al., 2019) and Ahmedabad (Rajesh and Ramachandran, 2017), among others. These variations in eBC levels vary in intensity, indicating that the daily changes in eBC content are strongly influenced by local emissions and meteorological factors.20

4.2. Spectral variation of absorption coefficient

Fig. 8 shows the seasonal mean spectral variation of absorption coefficients which exhibit a consistent and pronounced dependency at all wavelengths throughout all seasons. In general, the b_{abs} were found to be highest during the winter season while lowest in the monsoon season for all seven wavelengths. A large difference has occurred in absorption coefficients for the shorter wavelengths region than for the longer wavelengths. More specifically, at 880 nm winter season shows the highest b_{abs} value ($47.88 \pm 28.27 \text{ M m}^{-1}$) followed by summer ($38.93 \pm 27.85 \text{ M m}^{-1}$), post-monsoon ($29.22 \pm 20.54 \text{ M m}^{-1}$), and monsoon ($11.88 \pm 7.91 \text{ M m}^{-1}$) seasons. Such a seasonal variation in b_{abs} values at all wavelengths over the study site is mainly due to varying anthropogenic activities, their intensities, and seasonally changing local meteorological conditions (Gogoi et al., 2013). During the winter season, at a shorter wavelength particularly 370 nm, b_{abs} value enhanced abruptly and reached almost twice the value of post-monsoon and 1.54 times the value of summer season suggesting a significant contribution

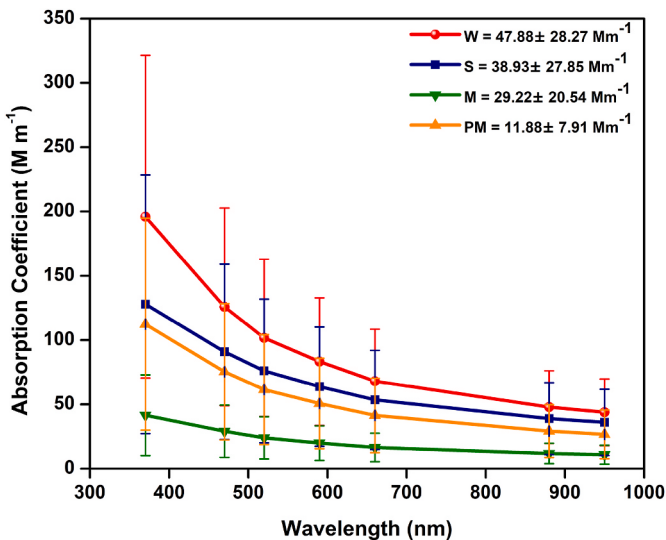


Fig. 8. Spectral variation of seasonal mean absorption coefficient over the study region.

of biomass burning aerosols during the winter and pre-monsoon season. In more detail, b_{abs} at 370 nm wavelength are found higher ~76%, 70%, 71%, and 74%, as compared to b_{abs} at 880 nm wavelength during winter, summer, monsoon, and post-monsoon seasons respectively. A higher value of b_{abs} at 370 nm wavelength is mainly caused by the emissions of local biomass burning. The increased burning of agricultural waste and the inflow of air masses from continental regions during summer elevate absorption coefficients. Monsoon periods show lower b_{abs} values due to the wet scavenging effect, which primarily accounts for the diminished b_{abs} values observed.

4.3. Season-wise diurnal variation of eBC, AAE, and BLH

Fig. 9 illustrates the diurnal patterns of total eBC, eBC_{ff} , eBC_{bb} concentrations, AAE₄₇₀₋₈₈₀, and BLH throughout the seasons. In each season, there are distinct morning and evening peaks, occurring approximately at 07:00–08:00 and 20:00–22:00 local time, respectively with a peak value of $9.2 \pm 4.8 \mu\text{g m}^{-3}$ (at lowest BLH 0.058 km) during winter, $8.2 \pm 4.7 \mu\text{g m}^{-3}$ (at BLH 0.128 km) during summer, $2.3 \pm 1.6 \mu\text{g m}^{-3}$ (at BLH 0.264 km) during monsoon, and $6.3 \pm 3.9 \mu\text{g m}^{-3}$ (at BLH 0.078 km) during post-monsoon. During the afternoon as the temperature rises, the atmospheric boundary layer height increases due to thermal convection and increased wind strength, resulting in reduced eBC levels during the daytime at 14:00–16:00 with a minimum value of $3.1 \pm 1.8 \mu\text{g m}^{-3}$ (at highest BLH of 1.169 km) in winter, $2.2 \pm 1.1 \mu\text{g m}^{-3}$ (at BLH of 1.967 km) in summer, $0.9 \pm 0.4 \mu\text{g m}^{-3}$ (at BLH of 0.957 km) during monsoon, and $1.8 \pm 0.8 \mu\text{g m}^{-3}$ (at BLH of 1.232 km) during post-monsoon season. During the cold season, there were many instances of severe pollution. These incidents occurred due to a combination of a stable boundary layer height (BLH) and a substantial temperature inversion (Ding et al., 2019). The figure displays a gradual eBC accumulation leading to a morning peak after sunrise, which can be attributed to the fumigation process as described by Stull (1988). Following sunset, the eBC mass concentration starts rising again due to decreased vertical convection and a shallower atmospheric boundary layer. Notably, the evening peak consistently surpasses the morning peak at the measurement location for all seasons. During the night, the boundary layer near the surface acts as an inversion, trapping eBC aerosols and causing their concentration to increase. This implies a more substantial influence of the boundary layer on the daily changes in eBC aerosols compared to their seasonal behavior. Kumar et al. (2020) reported the seasonal variation of eBC concentration during 2016-18 at Varanasi such as $10.857 \pm 6.991 \mu\text{g m}^{-3}$ during winter, $11.839 \pm 4.813 \mu\text{g m}^{-3}$ during summer, $4.593 \pm 2.225 \mu\text{g m}^{-3}$ during monsoon, and $8.924 \pm 5.319 \mu\text{g m}^{-3}$ during post-monsoon. Dumka et al. (2018)

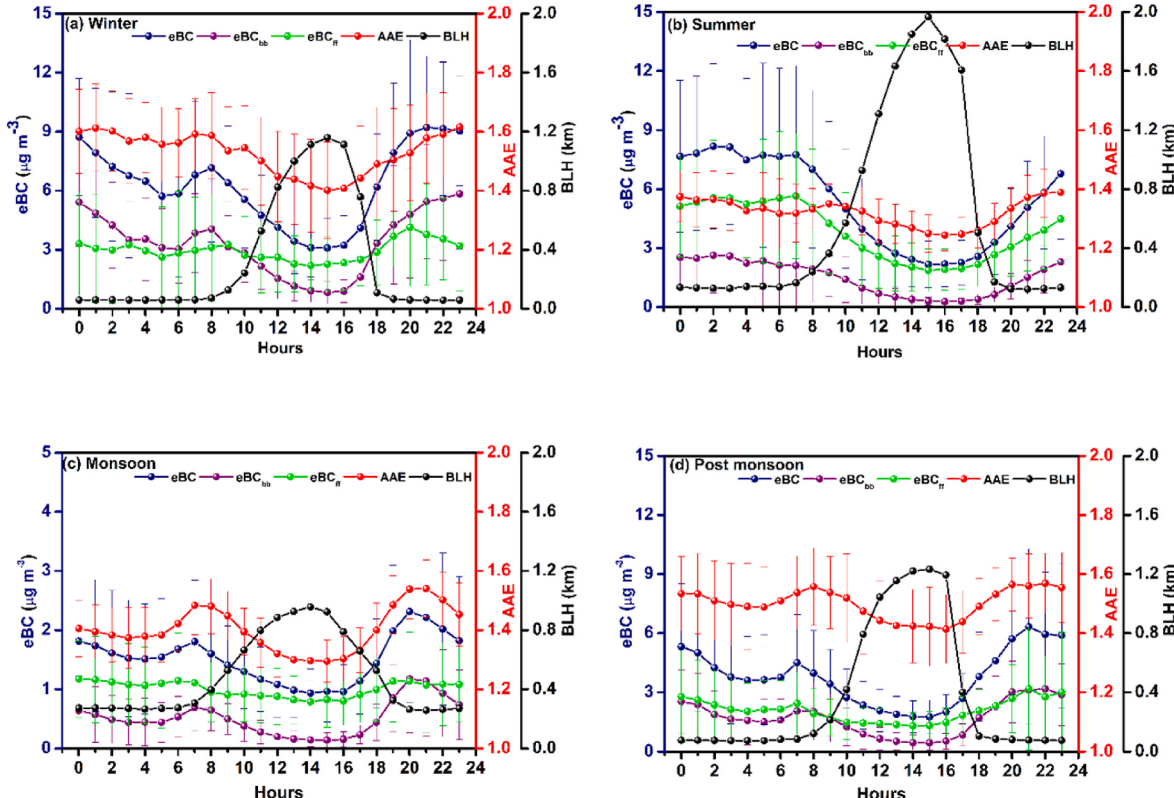


Fig. 9. Season-wise diurnal variation of eBC, eBC_{ff} , eBC_{bb} , AAE, and BLH during the study period over Varanasi.

reported the concentrations of eBC over Delhi which were low in summer ($4.6 \pm 0.2 \mu\text{g m}^{-3}$) and high in winter ($9.3 \pm 0.7 \mu\text{g m}^{-3}$) season. Bansal et al. (2019) suggest that the high concentration of eBC during the post-monsoon season results from widespread crop residue combustion in agricultural fields. More human activity in this area, such as the use of wood or biofuel for cooking, could also lead to an increase in eBC (Venkataraman et al., 2005). The winter season is recognized for stagnant climatic conditions, frequent burning processes against the cold weather, and man-made activities that induce the emission of small particulates and significant consequences of aerosols, including eBC (Dumka et al., 2013; Nair et al., 2007; Safai et al., 2007).

Seasonal AAE was generally higher during the post-monsoon and winter seasons, and lower in the summer and monsoon seasons, following the order: winter (1.53 ± 0.15) > post-monsoon (1.50 ± 0.12) > monsoon (1.40 ± 0.09) > summer (1.32 ± 0.08). Two prominent peaks were detected: one in the morning (07:00–08:00) and another in the evening (20:00–22:00), substantiating the dual impact of fossil fuel and biomass combustion during these time frames. Singh et al. (2015) also documented comparable AAE values over Varanasi for all seasons, specifically post-monsoon (1.11 ± 0.10), winter (1.02 ± 0.10), monsoon (1.01 ± 0.10), and summer (0.98 ± 0.10).

4.4. Relationship between AAE and components of eBC concentration

Fig. S1 provides supporting evidence for the significant correlation between the calculated AAE values and the estimated ratios of $\text{eBC}_{\text{ff}}/\text{eBC}_{\text{bb}}$ at two wavelengths (470 and 880 nm). The findings indicate a correlation between AAE and $\text{eBC}_{\text{ff}}/\text{eBC}_{\text{bb}}$, following a power law declining trend in both wavelength bands. The $\text{eBC}_{\text{ff}}/\text{eBC}_{\text{bb}}$ ratio exhibits significant variation, ranging from around 2 to 10 or higher, for AAE values between 1.24 and 1.5. This large range suggests a predominant contribution from fossil-fuel burning. However, for AAE values greater than 1.5, the $\text{eBC}_{\text{ff}}/\text{eBC}_{\text{bb}}$ ratio remains steady (below 1). This suggests that it is crucial to provide a precise definition of the AAE value to ensure the credibility of eBC source apportionment and the determination of the eBC_{ff} and eBC_{bb} fractions (Diapouli et al., 2017; Titos et al., 2017). The value of $\text{eBC}_{\text{ff}}/\text{eBC}_{\text{bb}}$ surpasses 13 when the AAE is 1.24 but tends towards zero as the AAE approaches 1.8. This discrepancy can be attributed to the greater influence of absorbing substances emitted from biomass burning at shorter wavelengths. According to Eck et al. (2005), the findings indicate that the Absorption Ångström Exponent (AAE) plays a crucial role in identifying the origin and characteristics of the aerosols responsible for absorption.

The monthly average fluctuation of AAE, as well as the respective

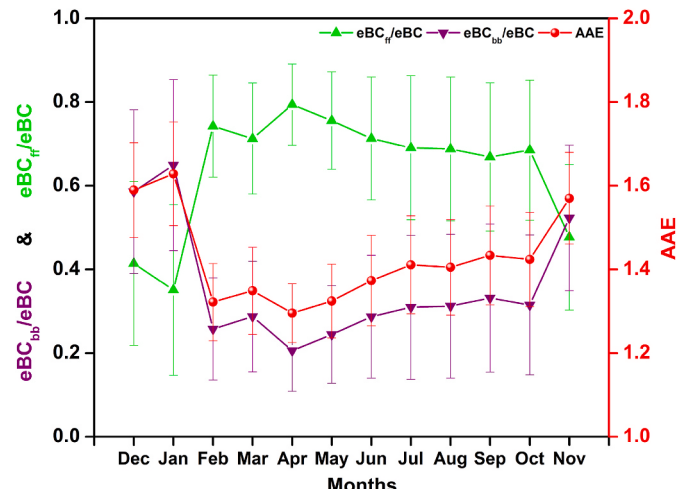


Fig. 10. Monthly mean variation of the contribution of eBC_{ff} & eBC_{bb} in total eBC concentrations and AAE over Varanasi.

contributions of eBC_{ff} and eBC_{bb} to the overall eBC, are depicted in Fig. 10. The study reveals that eBC_{ff} makes a higher contribution to eBC during the summer months (0.79 ± 0.09) with the lowest AAE (1.29 ± 0.07), which can be attributed to the dominance of fossil fuel combustion processes in eBC emissions. On the other hand, eBC_{bb} demonstrates its highest contribution during the winter months, particularly in January (0.65 ± 0.20) with the highest value of AAE (1.63 ± 0.12), primarily due to an increase in biomass combustion, relatively higher burning of wood for heating and culinary purposes. eBC_{bb} exhibits a similar pattern to that of AAE, while eBC_{ff} demonstrates an inverse relationship with AAE throughout the year.

4.5. Relationship between meteorological parameter and eBC concentration

Meteorological parameters like wind speed (WS, ms^{-1}), relative humidity (RH, %), and air temperature (Temp, $^{\circ}\text{C}$) play a vital role in the variation of boundary layer height (BLH, km) and atmospheric pollutants including eBC. Thus, the effect of the hourly correlation of meteorological parameters with eBC is investigated on a seasonal basis and the relationship is shown in Fig. 11. A strong negative correlation is found between eBC and temperature (Fig. 11a) with maximum correlation during summer ($r = -0.92$) followed by monsoon ($r = -0.72$), post-monsoon ($r = -0.69$) and winter months ($r = -0.69$). The negative correlation suggests that as the temperature increases, the levels of eBC tend to decrease, and vice versa which aids in understanding the interplay between temperature and eBC concentrations throughout the different climatic periods. A decrease in surface temperature during the winter season causes the accumulation of pollutants in the atmosphere resulting in higher concentrations of eBC while lower concentrations during the summer season are mainly due to the dispersion of pollutants because of relatively higher temperatures and strong winds. A negative correlation between temperature and eBC is also reported over the different regions of IGB (Bibi et al., 2017; Tiwari et al., 2013) and other regions of the world (Cao et al., 2009; Kucbel et al., 2017). On the other hand, a strong positive correlation between RH (%) ($<70\%$) and eBC mass concentration is found which is maximum for the summer season ($r = 0.96$) followed by the monsoon ($r = 0.73$), winter ($r = 0.71$) and post-monsoon ($r = 0.68$) season (Fig. 11b). A positive correlation suggests that a humid condition has a strong affinity towards eBC concentration and helps for hygroscopic growth of eBC and other pollutants that facilitate the dispersion process into the atmosphere (Liu et al., 2013). A positive correlation between RH and eBC concentration is also reported over the different regions of the world (Liu et al., 2018; Rajeevan et al., 2018). However, a few researchers also found a negative correlation between RH and eBC concentration in Karachi during 2006–2008 (Bibi et al., 2017) and over an Antarctic region (Botsa et al., 2021). Interestingly, for higher RH values ($>70\%$, except in monsoon where $\text{RH} > 75\%$) a reduction in eBC mass concentration is found which could be due to wet scavenging processes after the enhanced size of eBC particles because of hygroscopic growth (Ding et al., 2023). A negative correlation is found between WS and eBC concentration for all seasons with maximum value during winter ($r = -0.83$) followed by monsoon ($r = -0.81$), post-monsoon ($r = -0.79$), and summer season ($r = -0.77$) (Fig. 11c) suggesting a higher concentration of eBC under low wind speed condition and vice versa. Results suggest that during high wind conditions (particularly in the summer season), eBC aerosol produced from local sources may be transported to the nearby region while weaker wind during winter and post-monsoon season causes a reduction in atmospheric ventilation resulting in higher eBC near the surface. A negative correlation between eBC and wind speed is also reported by others (Bibi et al., 2017; Liu et al., 2018; Srivastava et al., 2012). As expected, a negative correlation is also found between BLH and eBC during all seasons with maximum value during monsoon ($r = -0.94$) followed by winter ($r = -0.89$), post-monsoon ($r = -0.85$) and summer season ($r = -0.78$) (Fig. 11d). These results are like earlier reported

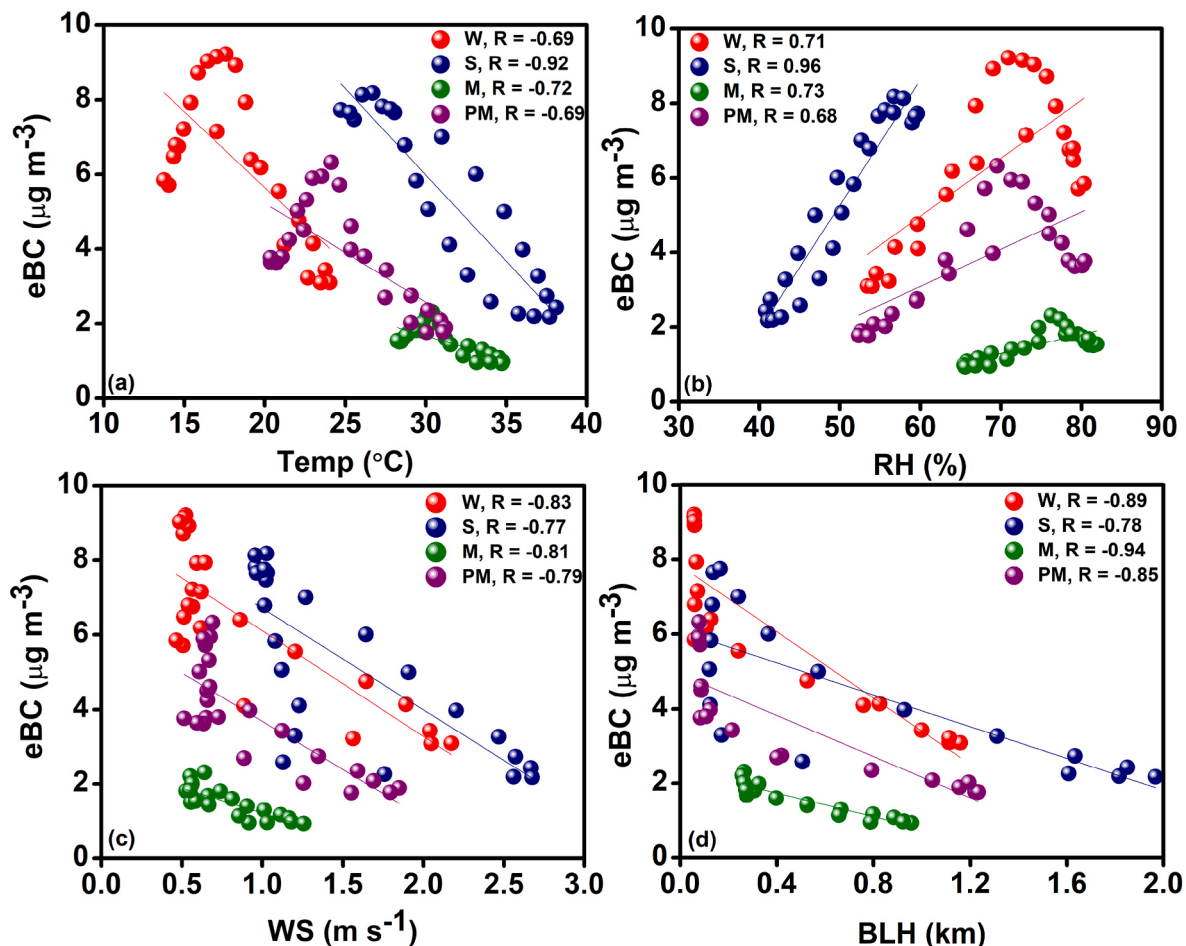


Fig. 11. Correlation of eBC with (a) temp, (b) RH, (c) WS, and (d) BLH for different seasons Winter (W), Summer (S), Monsoon (M), and Post monsoon (PM).

(Aruna et al., 2013; Liu et al., 2018; Rajeevan et al., 2018 and reference therein). The lower boundary layer during the winter season inhibits the dispersion and staged eBC particles into the atmosphere resulting in the highest eBC concentration. In other words, a higher concentration of eBC in the atmosphere enhances atmospheric stability and suppresses atmospheric turbulence which favors a low BLH.

4.6. Possible source identification and long-range transportation of BC

MODIS-derived fire count is a good proxy for biomass burning activities and the higher value of fire count over the region suggests intense biomass burning activities over the region and vice versa. Long-range transportation plays a vital role in eBC loading over any receptor site. Thus, to investigate the possible source region and long-range transportation of BC, five-day air mass back trajectories were computed at three distinct altitudes (500, 100, and 1500 m AGL) (Ravindra et al., 2019; Rolph et al., 2017) using NCEP/NCAR global reanalysis wind dataset as input. These daily airmass back trajectories are superimposed over MODIS-derived total fire counts on a seasonal basis. (Fig. S2). MODIS fire counts reflect that during the winter season, relatively higher fire counts are observed over the IGB region, and air masses are mainly reached at the receptor site through the IGB region resulting in the highest eBC concentration during winter months. At lower altitudes (500 m AGL), air masses are mainly coming from Afghanistan and Pakistan via IGB while at higher altitudes, air masses are coming from Iran, Turkmenistan, and Uzbekistan following mostly the same path over IGB. Long-range transportation of particulate matter over Varanasi during the winter season was also reported in the earlier study (Kumar et al., 2015; Singh et al., 2014). During pre-monsoon

season, the high fire count density is found over the IGB region suggesting the highest biomass burning activity and the majority of air-masses reached at receptor sites at all three different altitudes comes through the IGB region. In contrast, during the post-monsoon season a dense fire count is found over the northern IGB (Haryana and Punjab) which is mainly attributed to intense crop-residue burning and combined with north-westerly winds helps air masses to bring biomass-burning aerosol over receptor sites (Kaskaoutis et al., 2014; Kharol et al., 2012). To investigate the possible contribution of different regions in eBC loading, we further performed cluster analysis by following the total spatial variance method, using daily individual air-mass back trajectories (at 1000 m AGL) as input as shown in Fig. 12. The figure reflects that during the post-monsoon and winter seasons, the northwestern part of the IGB region is the major contributor to polluted air masses at the receptor site. A significant contribution of arid land airmasses is also found at Varanasi i.e. (i.e. 20 % for winter and 31 % for post-monsoon season) passing through the IGB region suggesting the occurrence of polluted black carbon (brown carbon) over Varanasi. In addition, interestingly during the summer season, central India and IGB have nearly similar contributions in polluted air mass loading over the receptor site. On the other hand, during monsoon season, Varanasi experiences nearly equal oceanic and land air masses.

5. Conclusions

In this study, one year (Dec. 2020–Nov. 2021) continuous and high temporal resolution of surface eBC concentration is measured using an Aethalometer (AE-33) to investigate the temporal variation in eBC mass concentration and its source apportionment. In addition to this, the

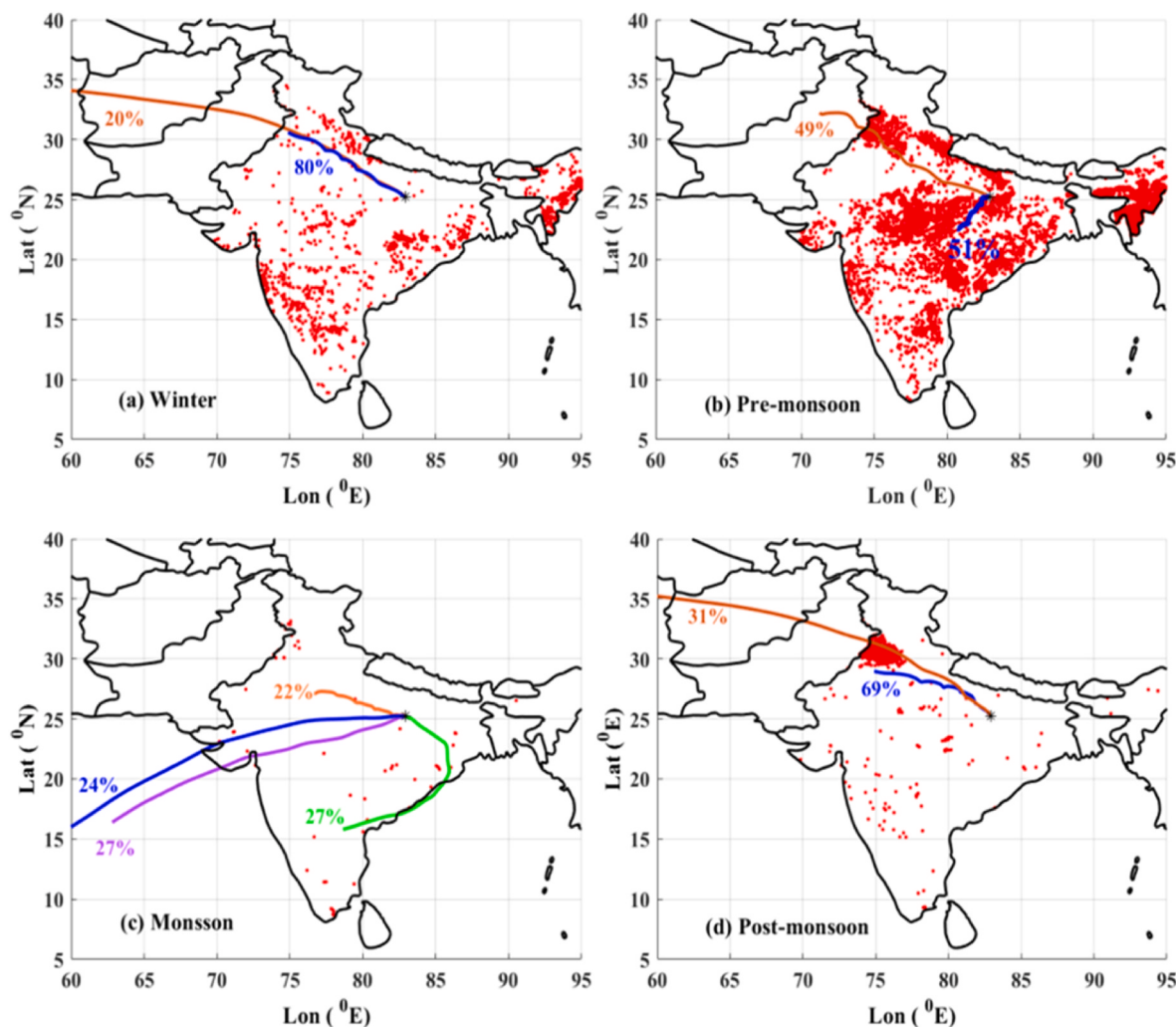


Fig. 12. Seasonal variation of MODIS fire counts and five-day airmass backward trajectories along with their contribution.

impact of regional meteorological conditions on surface eBC mass concentration during different seasons and long-range transportation patterns of eBC have been also studied. The key findings of the present study are summarized as follows.

- eBC concentration shows a large variation range between 0.46 ± 0.13 to $11.22 \pm 5.09 \mu\text{g m}^{-3}$ with annual mean $\sim 3.57 \pm 2.39 \mu\text{g m}^{-3}$ during the study period associated with a well-defined diurnal variation with two different maxima between 07:00–08:00 and 20:00–22:00. The highest morning peak ($13.79 \pm 7.04 \mu\text{g m}^{-3}$) is observed during February month while the lowest ($0.74 \pm 0.24 \mu\text{g m}^{-3}$) is during August month.
- The monthly mean eBC concentration is found maximum during February ($6.63 \pm 3.61 \mu\text{g m}^{-3}$), closely followed by March ($6.42 \pm 3.93 \mu\text{g m}^{-3}$) and minimum ($1.34 \pm 0.82 \mu\text{g m}^{-3}$) in July month whereas on seasonal basis, highest eBC concentration is observed during winter ($6.21 \pm 3.56 \mu\text{g m}^{-3}$) followed by summer ($5.09 \pm 3.61 \mu\text{g m}^{-3}$) and minimum in monsoon season ($1.52 \pm 1.03 \mu\text{g m}^{-3}$).
- The daily mean eBC mass concentration shows a negative correlation with all meteorological parameters (temperature, wind speed, and boundary layer height) except relative humidity which shows a positive correlation with eBC mass concentration. The mean mass concentration of eBC increases with respect to RH (up to 70 %, except during monsoon season where RH is up to 75 %) suggesting hygroscopic growth while for higher RH (>70 %) value, eBC

concentration decreases and indicates the possible wet scavenging process of BC into the atmosphere.

- Source apportionment of eBC using the “Aethalometer Model” reveals that eBC_{ff} is dominant over eBC_{bb} in total eBC loading during the study period.
- Investigations utilizing MODIS fire counts and cluster analysis of airmass back trajectories revealed that IGB could be a significant source for the black carbon loading over the study region.

CRediT authorship contribution statement

Prashant Kumar Chauhan: Formal analysis, Plotting graphs, Data curation, Writing – original draft. **Shani Tiwari:** Writing – review & editing, Plotting, Writing – review & editing. **Dileep Kumar Gupta:** Computation, Writing – review & editing. **Akhilesh Kumar:** Formal analysis, plotting. **Vineet Pratap:** Writing – review & editing. **Abhay Kumar Singh:** Writing – review & editing, Conceptualization, Supervision, Writing – review & editing.

Declaration of competing interest

The authors declare that they have no known competing financial interests or personal relationships that could have appeared to influence the work reported in this paper.

Acknowledgment

This work is partially supported by the Institute of Eminence (IoE) to BHU Scheme No. 6031. One of the Authors, PKC is thankful to the University Grant Commission, New Delhi for providing a Junior Research Fellowship. Author Shani Tiwari is thankful to the Director, CSIR- National Institute of Oceanography (CSIR-NIO) for providing the basic facilities to carry out the research. We are also thankful to all three anonymous reviewers for their positive feedback/suggestions which improve the content of the manuscript. The NIO contribution number is 7188.

Appendix A. Supplementary data

Supplementary data to this article can be found online at <https://doi.org/10.1016/j.apr.2024.102061>.

References

- Ambade, B., Sankar, T.K., Kumar, A., Gautam, A.S., Gautam, S., 2021. COVID-19 lockdowns reduce the Black carbon and polycyclic aromatic hydrocarbons in the Asian atmosphere: source apportionment and health hazard evaluation. *Environ. Dev. Sustain.* 23, 12252–12271. <https://doi.org/10.1007/s10668-020-01167-1>.
- Aruna, K., Kumar, T.L., Rao, D.N., Murthy, B.K., Babu, S.S., Moorthy, K.K., 2013. Black carbon aerosols in a tropical semi-urban coastal environment: effects of boundary layer dynamics and long-range transport. *J. Atmos. Sol. Terr. Phys.* 104, 116–125.
- Babu, K. V. Suresh, Roy, Arijit, Ramachandra Prasad, P., 2016. Developing the static fire Danger Index using Geospatial Technology. Proceedings of the 2016 2nd International Conference on Contemporary Computing and Informatics IC3I, 558–563. <https://doi.org/10.1109/IC3I.2016.7918026>, 2016.
- Bansal, O., Singh, A., Singh, D., 2019. Characteristics of Black Carbon aerosols over Patiala Northwestern part of the IGP: source apportionment using cluster and CWT analysis. *Atmos. Pollut. Res.* 10, 244–256. <https://doi.org/10.1016/j.apr.2018.08.001>.
- Bibi, S., Alam, K., Chishtie, F., Bibi, H., Rahman, S., 2017. Temporal variation of Black Carbon concentration using Aethalometer observations and its relationships with meteorological variables in Karachi, Pakistan. *J. Atmos. Sol. Terr. Phys.* 157, 67–77.
- Bond, T.C., Doherty, S.J., Fahey, D.W., Forster, P.M., Bernsten, T., Deangelo, B.J., Flanner, M.G., Ghan, S., Kärcher, B., Koch, D., Kinne, S., Kondo, Y., Quinn, P.K., Sarofim, M.C., Schultz, M.G., Schulz, M., Venkataraman, C., Zhang, H., Zhang, S., Bellouin, N., Guttikunda, S.K., Hopke, P.K., Jacobson, M.Z., Kaiser, J.W., Klimont, Z., Lohmann, U., Schwarz, J.P., Shindell, D., Storelvmo, T., Warren, S.G., Zender, C.S., 2013. Bounding the role of black carbon in the climate system: a scientific assessment. *J. Geophys. Res. Atmos.* 118, 5380–5552. <https://doi.org/10.1002/jgrd.50171>.
- Botsa, S.M., Tara, D.L.L.M., Magesh, N.S., Tiwari, A.K., 2021. Characterization of black carbon aerosols over Indian Antarctic station, Maitri and identification of potential source areas. *Environ. sci. Atmos.* 1 (6), 416–422.
- Cao, J.J., Zhu, C.S., Chow, J.C., Watson, J.G., Han, Y.M., Wang, G.H., Shen, Z.X., An, Z. S., 2009. Black carbon relationships with emissions and meteorology in Xian, China. *Atmos. Res.* 94 (2), 194–202.
- Census of India, 2011. Office of the Registrar General & Census Commissioner. Ministry of Home Affairs, GoI. <http://censusindia.gov.in/2011-common/CensusData2011.html>.
- Chen, B., Andersson, A., Lee, M., Kirillova, E.N., Xiao, Q., Kruså, M., Shi, M., Hu, K., Lu, Z., Streets, D.G., Du, K., Gustafsson, Ö., 2013. Source forensics of black carbon aerosols from China. *Environ. Sci. Technol.* 47, 9102–9108. <https://doi.org/10.1021/es401599r>.
- Chowdhury, Ehsan H., Hassan, Quazi K., 2015. Development of a New daily-scale forest fire danger forecasting system using remote sensing data. *Rem. Sens.* 7 (3), 2431–2448. <https://doi.org/10.3390/rs70302431>.
- Dasgupta, P., Srikanth, K., 2020. Reduced air pollution during COVID-19: learnings for sustainability from Indian Cities. *Glob. Transit.* 2, 271–282.
- Diapouli, E., Kalogridis, A.C., Markantonaki, C., Vratolis, S., Petfatzis, P., Colombi, C., Eleftheriadis, K., 2017. Annual variability of black carbon concentrations originating from biomass and fossil fuel combustion for the suburban aerosol in Athens, Greece. *Atmosphere* 8, 234. <https://doi.org/10.3390/atmos8120234>.
- Ding, S., Liu, D., Zhao, D., Hu, K., Tian, P., Zhou, W., Huang, M., Yang, Y., Wang, F., Sheng, J., Liu, Q., 2019. Size-related physical properties of black carbon in the lower atmosphere over Beijing and Europe. *Environ. Sci. Technol.* 53 (19), 11112–11121. <https://doi.org/10.1021/acs.est.9b03722>.
- Ding, S., Liu, D., Zhao, D., Tian, P., Huang, M., Ding, D., 2023. Characteristics of atmospheric black carbon and its wet scavenging in Nanning, South China. *Sci. Total Environ.* 904, 166747 <https://doi.org/10.1016/j.scitotenv.2023.166747>.
- Dumka, U.C., Kaskaoutis, D.G., Tiwari, S., Safai, P.D., Attri, S.D., Soni, V.K., Singh, N., Mihalopoulos, N., 2018. Assessment of biomass burning and fossil fuel contribution to black carbon concentrations in Delhi during winter. *Atmos. Environ.* 194, 93–109. <https://doi.org/10.1016/j.atmosenv.2018.09.033>.
- Dumka, U.C., Manchanda, R.K., Sinha, P.R., Sreenivasan, S., Moorthy, K.K., Suresh Babu, S., 2013. Temporal variability and radiative impact of black carbon aerosol over tropical urban station Hyderabad. *J. Atmos. Sol. Terr. Phys.* 105–106, 81–90. <https://doi.org/10.1016/j.jastp.2013.08.003>.
- Dumka, U.C., Moorthy, K.K., Kumar, A., Hegde, P., Sagar, R., Pant, P., Singh, N., Babu, S. S., 2010. Characteristics of aerosol black carbon mass concentration over a high altitude location in the Central Himalayas from multi-year measurements. *Atmos. Res.* 96, 510–521. <https://doi.org/10.1016/j.atmosres.2009.12.010>.
- Eck, T.F., Holben, B.N., Dubovik, O., Smirnov, A., Goloub, P., Chen, H.B., Chatenet, B., Gomes, L., Zhang, X.Y., Tsay, S.C., Ji, Q., Giles, D., Slutsker, I., 2005. Columnar aerosol optical properties at AERONET sites in central eastern Asia and aerosol transport to the tropical mid-Pacific. *J. Geophys. Res. Atmos.* 110, 1–18. <https://doi.org/10.1029/2004JD005274>.
- Favez, O., El Haddad, I., Piot, C., Boréave, A., Abidi, E., Marchand, N., Jaffrezo, J.L., Besombes, J.L., Personnaz, M.B., Sciaire, J., Wortham, H., George, C., D'Anna, B., 2010. Inter-comparison of source apportionment models for the estimation of wood burning aerosols during wintertime in an Alpine city (Grenoble, France). *Atmos. Chem. Phys.* 10, 5295–5314. <https://doi.org/10.5194/acp-10-5295-2010>.
- Giglio, L., Kendall, J.D., Mack, R., 2003. A multi-year active fire dataset for the tropics derived from the TRMM VIRS. *Int. J. Rem. Sens.* 24, 4505–4525. <https://doi.org/10.1080/0143116031000070283>.
- Goel, V., Hazarika, N., Kumar, M., Singh, V., Thamban, N.M., Tripathi, S.N., 2021. Variations in Black Carbon concentration and sources during COVID-19 lockdown in Delhi. *Chemosphere* 270, 129435. <https://doi.org/10.1016/j.chemosphere.2020.129435>.
- Gogoi, M.M., Suresh Babu, S., Krishna Moorthy, K., Manoj, M.R., Chaubey, J.P., 2013. Absorption characteristics of aerosols over the northwestern region of India: distinct seasonal signatures of biomass burning aerosols and mineral dust. *Atmos. Environ.* 73, 92–102. <https://doi.org/10.1016/j.atmosenv.2013.03.009>.
- Gupta, P., Jangid, A., Kumar, R., 2023. COVID-19-associated 2020 lockdown: a study on atmospheric black carbon fall impact on human health. *Environ. Geochem. Health* 45, 3507–3520. <https://doi.org/10.1007/s10653-022-01430-6>.
- Gustafsson, O., Krusa, M., Zencak, Z., Sheesley, R.J., Granat, L., Engstrom, E., Praveen, P. S., Rao, P.S.P., Leck, C., Rodhe, H., 2009. Brown clouds over South Asia: biomass or fossil fuel combustion? *Science* 323, 495–498.
- Hansen, J., Sato, M., Ruedy, R., Nazarenko, L., Lacis, A., Schmidt, G.A., Russell, G., Aleinov, I., Bauer, M., Bauer, S., Bell, N., Cairns, B., Canuto, V., Chandler, M., Cheng, Y., Del Genio, A., Faluvegi, G., Fleming, E., Friend, A., Hall, T., Jackman, C., Kelley, M., Kiang, N., Koch, D., Lean, J., Lerner, J., Lo, K., Menon, S., Miller, R., Minnis, P., Novakov, T., Oinas, V., Perlitz, Ja, Perlitz, Ju, Rind, D., Romanou, A., Shindell, D., Stone, P., Sun, S., Tausnev, N., Thresher, D., Wielicki, B., Wong, T., Yao, M., Zhang, S., 2005. Efficacy of climate forcings. *J. Geophys. Res. Atmos.* 110 <https://doi.org/10.1029/2005JD005776>.
- Herich, H., Hueglin, C., Buchmann, B., 2011. A 2.5 year's source apportionment study of black carbon from wood burning and fossil fuel combustion at urban and rural sites in Switzerland. *Atmos. Meas. Tech.* 4, 1409–1420. <https://doi.org/10.5194/amt-4-1409-2011>.
- Hong, X., Zhang, C., Tian, Y., Wu, H., Zhu, Y., Liu, C., 2023. Quantification and evaluation of atmospheric emissions from crop residue burning constrained by satellite observations in China during 2016–2020. *Sci. Total Environ.* 865, 161237.
- Hussain, A.J., Sankar, T.K., Vithanage, M., Ambade, B., Gautam, S., 2023. Black carbon emissions from traffic contribute sustainability to air pollution in urban cities of India. *Water Air Soil Pollut.* 234, 217. <https://doi.org/10.1007/s11270-023-06232-9>.
- Janssen, N.A., Gerlofs-Nijland, M.E., Lanki, T., Salonen, R.O., Cassee, F., Hoek, G., Fischer, P., Brunekreef, B., Krzyzanowski, M., 2012. Health Effects of Black Carbon. World Health Organization.
- Jethva, H., 2022. Assessing predictability of post-monsoon crop residue fires in Northwestern India. *Front. Earth Sci.* 10, 2473.
- Jing, A., Zhu, B., Wang, H., Yu, X., An, J., Kang, H., 2019. Source apportionment of black carbon in different seasons in the northern suburb of Nanjing, China. *Atmos. Environ.* 201, 190–200. <https://doi.org/10.1016/j.atmosenv.2018.12.060>.
- Joshi, H., Naja, M., Singh, K.P., Kumar, R., Bhardwaj, P., Babu, S.S., Satheesh, S.K., Moorthy, K.K., Chandola, H.C., 2016. Investigations of aerosol black carbon from a semi-urban site in the Indo-Gangetic Plain region. *Atmos. Environ.* 125, 346–359. <https://doi.org/10.1016/j.atmosenv.2015.04.007>.
- Justice, C.O., Giglio, L., Korontzi, S., Owens, J., Morisette, J.T., Roy, D., Descloitres, J., Alleaume, S., Petitcolin, P., Kaufman, Y., 2002. The MODIS fire products. *Remote Sens. Environ.* 83 (1–2), 244–262.
- Kanawade, V.P., Tripathi, S.N., Bhattu, D., Shamjad, P.M., 2014. Sub-micron particle number size distributions characteristics at an urban location, Kanpur, in the Indo-Gangetic Plain. *Atmos. Res.* 147–148, 121–132. <https://doi.org/10.1016/j.atmosres.2014.05.010>.
- Kant, Y., Chauhan, P., Natwariya, A., Kannaujiya, S., Mitra, D., 2022. Long term influence of groundwater preservation policy on stubble burning and air pollution over North-West India. *Sci. Rep.* 12, 2090. <https://doi.org/10.1038/s41598-022-06043-8>.
- Kaskaoutis, D.G., Kumar, S., Sharma, D., Singh, R.P., Kharol, S.K., Sharma, M., Singh, A. K., Singh, S., Singh, A., Singh, D., 2014. Effects of crop residue burning on aerosol properties, plume characteristics, and long-range transport over northern India. *J. Geophys. Res. Atmos.* 119 (9), 5424–5444.
- Kaur, P., Srinivasan, P., Dhar, P., Kumar De, B., Guha, A., 2020. Study of spectral characteristics of black carbon from biomass burning and source apportionment over Agartala in the northeastern India. *Environ. Sci. Pollut. Res.* 27, 16584–16598. <https://doi.org/10.1007/s11356-020-08094-8>.
- Kharol, S.K., Badarinath, K.V.S., Sharma, A.R., Mahalakshmi, D.V., Singh, D., Prasad, V. K., 2012. Black carbon aerosol variations over Patiala city, Punjab, India—a study

- during agriculture crop residue burning period using ground measurements and satellite data. *J. Atmos. Sol. Terr. Phys.* 84, 45–51.
- Kiran, V.R., Talukdar, S., Ratnam, M.V., Jayaraman, A., 2018. Long-term observations of black carbon aerosol over a rural location in southern peninsular India: role of dynamics and meteorology. *Atmos. Environ.* 189, 264–274.
- Klimont, Z., Kupiainen, K., Heyes, C., Purohit, P., Cofala, J., Rafaj, P., Borken-Kleefeld, J., Schöpp, W., 2017. Global anthropogenic emissions of particulate matter including black carbon. *Atmos. Chem. Phys.* 17, 8681–8723. <https://doi.org/10.5194/acp-17-8681-2017>.
- Kucbel, M., Corsaro, A., Švédová, B., Raclavská, H., Raclavský, K., Juchelková, D., 2017. Temporal and seasonal variations of black carbon in a highly polluted European city: apportionment of potential sources and the effect of meteorological conditions. *J. Environ. Manag.* 203, 1178–1189.
- Kumar, M., Tiwari, S., Murari, V., Singh, A.K., Banerjee, T., 2015. Wintertime characteristics of aerosols at middle Indo-Gangetic Plain: impacts of regional meteorology and long range transport. *Atmos. Environ.* 104, 162–175. <https://doi.org/10.1016/j.atmosenv.2015.01.014>.
- Kumar, R.R., Soni, V.K., Jain, M.K., 2020. Evaluation of spatial and temporal heterogeneity of black carbon aerosol mass concentration over India using three year measurements from IMD BC observation network. *Sci. Total Environ.* 723, 138060. <https://doi.org/10.1016/j.scitotenv.2020.138060>.
- Lodhi, N.K., Beegum, S.N., Singh, S., Kumar, K., 2013. Aerosol climatology at Delhi in the western Indo-Gangetic Plain: microphysics, long-term trends, and source strengths. *J. Geophys. Res. Atmos.* 118 (3), 1361–1375.
- Liu, B., Ma, Y., Gong, W., Zhang, M., Shi, Y., 2018. The relationship between black carbon and atmospheric boundary layer height. *Atmos. Pollut. Res.* 10 (1), 65–72.
- Liu, D., Allan, J., Whitehead, J., Young, D., Flynn, M., Coe, H., McFiggans, G., Fleming, Z., L., Bandy, B., 2013. Ambient black carbon particle hygroscopic properties controlled by mixing state and composition. *Atmos. Chem. Phys.* 13, 2015–2029.
- Malik, A., Aggarwal, S.G., Ohata, S., Mori, T., Kondo, Y., Sinha, P.R., Patel, P., Kumar, B., Singh, K., Soni, D., Koike, M., 2022. Measurement of black carbon in Delhi: evidences of regional transport, meteorology and local sources for pollution episodes. *Aerosol Air Qual. Res.* 22, 220128. <https://doi.org/10.4209/aaqr.220128>.
- Meena, G.S., Mukherjee, S., Buchunde, P., Safai, P.D., Singla, V., Aslam, M.Y., Sonbawne, S.M., Made, R., Anand, V., Dani, K.K., Pandithurai, G., 2021. Seasonal variability and source apportionment of black carbon over a rural high-altitude and an urban site in western India. *Atmos. Pollut. Res.* 12, 32–45. <https://doi.org/10.1016/j.apr.2020.10.006>.
- Mousavi, A., Sowlat, M.H., Lovett, C., Rauber, M., Szidat, S., Boffi, R., Borgini, A., De Marco, C., Ruprecht, A.A., Sioutas, C., 2019. Source apportionment of black carbon (BC) from fossil fuel and biomass burning in metropolitan Milan, Italy. *Atmos. Environ. Times* 203, 252–261.
- Murari, V., Kumar, M., Mhawish, A., Barman, S.C., Banerjee, T., 2017. Airborne particulate in Varanasi over middle Indo-Gangetic Plain: variation in particulate types and meteorological influences. *Environ. Monit. Assess.* 189, 1–15.
- Nair, V.S., Moorthy, K.K., Alappattu, D.P., Kunhikrishnan, P.K., George, S., Nair, P.R., Babu, S.S., Abish, B., Satheesh, S.K., Tripathi, S.N., Niranjana, K., Madhavan, B.L., Srikanth, V., Dutt, C.B.S., Badarinath, K.V.S., Reddy, R.R., 2007. Wintertime aerosol characteristics over the Indo-Gangetic Plain (IGP): impacts of local boundary layer processes and long-range transport. *J. Geophys. Res. Atmos.* 112. <https://doi.org/10.1029/2006JD008099>.
- Petzold, A., Ogren, J.A., Fiebig, M., Laj, P., Li, S.M., Baltensperger, U., Holzer-Popp, T., Kinne, S., Pappalardo, G., Sugimoto, N., Wehrli, C., 2013. Recommendations for reporting "black carbon" measurements. *Atmos. Chem. Phys.* 13 (16), 8365–8379.
- Rajeevan, K., Sumesh, R.K., Resmi, E.A., Unnikrishnan, C.K., 2018. An observational study on the variation of black carbon aerosol and source identification over a tropical station in south India. *Atmos. Pollut. Res.* 10 (1), 30–44.
- Rajesh, T.A., Ramachandran, S., 2017. Characteristics and source apportionment of black carbon aerosols over an urban site. *Environ. Sci. Pollut. Res.* 24, 8411–8424. <https://doi.org/10.1007/s11356-017-8453-3>.
- Rajesh, T.A., Ramachandran, S., 2022. Assessment of the coronavirus disease 2019 (COVID-19) pandemic imposed lockdown and unlock effects on black carbon aerosol, its source apportionment, and aerosol radiative forcing over an urban city in India. *Atmos. Res.* 267, 105924. <https://doi.org/10.1016/j.atmosres.2021.105924>.
- Rajesh, T.A., Ramachandran, S., Dhaker, V.K., 2021. Black carbon aerosols: relative source strengths of vehicular emissions and residential/open wood burning over an urban and a semi-urban environment. *Atmos. Pollut. Res.* 12, 101060. <https://doi.org/10.1016/j.apr.2021.101060>.
- Ramachandran, S., Rajesh, T.A., Cherian, R., 2021. Black carbon aerosols over source vs. background region: atmospheric boundary layer influence, potential source regions, and model comparison. *Atmos. Res.* 256, 105573. <https://doi.org/10.1016/j.atmosres.2021.105573>.
- Ramanathan, V., Carmichael, G., 2008. Global and regional climate changes due to black carbon. *Nat. Geosci.* 1, 221–227. <https://doi.org/10.1038/ngeo156>.
- Rana, A., Dey, S., Rawat, P., Mukherjee, A., Mao, J., Jia, S., Khillare, P.S., Yadav, A.K., Sarkar, S., 2020. Optical properties of aerosol brown carbon (BrC) in the eastern Indo-Gangetic Plain. *Sci. Total Environ.* 716, 137102. <https://doi.org/10.1016/j.scitotenv.2020.137102>.
- Rana, A., Rawat, P., Sarkar, S., 2023. Sources, transport pathways and radiative effects of BC aerosol during 2018–2020 at a receptor site in the eastern Indo-Gangetic Plain. *Atmos. Environ.* 309, 119900. <https://doi.org/10.1016/J.ATMOSENV.2023.119900>.
- Rathod, T.D., Sahu, S.K., 2022. Measurements of optical properties of black and brown carbon using multi-wavelength absorption technique at Mumbai, India. *J. Earth Syst. Sci.* 131 (1), 32.
- Ravindra, K., Singh, T., Mor, Sahil, Singh, V., Mandal, T.K., Bhatti, M.S., Gahlawat, S.K., Dhankhar, R., Mor, Suman, Beig, G., 2019. Real-time monitoring of air pollutants in seven cities of North India during crop residue burning and their relationship with meteorology and transboundary movement of air. *Sci. Total Environ.* 690, 717–729. <https://doi.org/10.1016/j.scitotenv.2019.06.216>.
- Rolph, G., Stein, A., Stunder, B., 2017. Real-time environmental applications and display system: ready. *Environ. Model. Software* 95, 210–228. <https://doi.org/10.1016/j.envsoft.2017.06.025>.
- Safai, P.D., Kewat, S., Praveen, P.S., Rao, P.S.P., Momin, G.A., Ali, K., Devara, P.C.S., 2007. Seasonal variation of black carbon aerosols over a tropical urban city of Pune, India. *Atmos. Environ.* 41, 2699–2709. <https://doi.org/10.1016/j.atmosenv.2006.11.044>.
- Sandradewi, J., Jisca, Prévôt, A.S.H., Szidat, S., Perron, N., Alfara, M.R., Lanz, V.A., Weingartner, E., Baltensperger, U.R.S., 2008a. Using aerosol light absorption measurements for the quantitative determination of wood burning and traffic emission contribution to particulate matter. *Environ. Sci. Technol.* 42, 3316–3323. <https://doi.org/10.1021/es702253m>.
- Sandradewi, J., Prévôt, A.S.H., Weingartner, E., Schmidhauser, R., Gysel, M., Baltensperger, U., 2008b. A study of wood burning and traffic aerosols in an Alpine valley using a multi-wavelength Aethalometer. *Atmos. Environ.* 42, 101–112. <https://doi.org/10.1016/j.atmosenv.2007.09.034>.
- Saikia, D.S., Kant, Y., Mitra, D., Singh, A., Chandola, H.C., Sateesh, M., Babu, S.S., Chauhan, P., 2019. Impact of biomass burning on regional aerosol optical properties: a case study over northern India. *J. Environ. Manag.* 244, 328–343. <https://doi.org/10.1016/j.jenvman.2019.04.025>.
- Singh, A.K., Srivastava, M.K., Singh, M., Srivastava, A., Kumar, S., Tiwari, Shani, Singh, B.P., Bisht, D.S., Tiwari, Suresh, 2014. Characterisation of atmospheric aerosol by SEM-EDX and ion-chromatography techniques for eastern indo-ganggetic plain location, Varanasi, India. *Int. J. Adv. Earth Sci.* 3, 41–51.
- Singh, B.P., Tiwari, S., Hopke, P.K., Singh, R.S., Bisht, D.S., Srivastava, A.K., Singh, R.K., Dumka, U.C., Singh, A.K., Rai, B.N., Srivastava, M.K., 2015. Seasonal inhomogeneity of soot particles over the central indo-ganggetic plains, India: influence of meteorology. *J. Meteorol. Res.* 29, 935–949. <https://doi.org/10.1007/s13351-015-5041-7>.
- Singh, N., Mhawish, A., Banerjee, T., Ghosh, S., Singh, R.S., Mall, R.K., 2021. Association of aerosols, trace gases and black carbon with mortality in an urban pollution hotspot over central Indo-Gangetic Plain. *Atmos. Environ.* 246, 118088. <https://doi.org/10.1016/j.atmosenv.2020.118088>.
- Singh, S., Gokhale, S., 2022. Effect of COVID-19 epidemic-led lockdowns on aerosol black carbon concentration, sources and its radiation effect in northeast India. *J. Earth Syst. Sci.* 131, 139. <https://doi.org/10.1007/s12040-022-01883-4>.
- Sivasankaran, G., Jayabalakrishnan, R.M., Maheswari, M., Kumaraperumal, R., 2022. Intra-seasonal and seasonal transition variation of aerosol Black Carbon over high altitude region of southern India. Ooty, Tamilnadu. *Pollut. Res.* 41, 328–334. <https://doi.org/10.53550/Pr.2022.V41i01.048>.
- Srivastava, A.K., Singh, S., Pant, P., Dumka, U.C., 2012. Characteristics of black carbon over Delhi and Manora Peak-a comparative study. *Atmos. Sci. Lett.* 13, 223–230. <https://doi.org/10.1002/asl.386>.
- Srivastava, R., Ramachandran, S., 2013. The mixing state of aerosols over the Indo-Gangetic Plain and its impact on radiative forcing. *Q. J. R. Meteorol. Soc.* 139, 137–151. <https://doi.org/10.1002/qj.1958>.
- Srivastava, S., Kumar, M., Singh, R.S., Rai, B.N., Mall, R.K., Banerjee, T., 2019. Long-term observation of black carbon aerosols at an urban location over the central Indo-Gangetic Plain, South Asia. *Atmosfera* 32, 95–113. <https://doi.org/10.20937/ATM.2019.32.02.02>.
- Stein, A.F., Draxler, R.R., Rolph, G.D., Stunder, B.J.B., Cohen, M.D., Ngan, F., 2015. NOAA's hysplit atmospheric transport and dispersion modeling system. *Bull. Am. Meteorol. Soc.* 96, 2059–2077. <https://doi.org/10.1175/BAMS-D-14-00110.1>.
- Stull, R.B., 1988. An Introduction to Boundary Layer Meteorology, vol. 13. Springer Science & Business Media.
- Taubman, B.F., Hains, J.C., Thompson, A.M., Marufu, L.T., Doddridge, B.G., Stehr, J.W., Piety, C.A., Dickerson, R.R., 2006. Aircraft vertical profiles of trace gas and aerosol pollution over the mid-Atlantic United States: statistics and meteorological cluster analysis. *J. Geophys. Res. Atmos.* 111 (D10).
- Titos, G., del Águila, A., Cazorla, A., Lyamani, H., Casquero-Vera, J.A., Colombi, C., Cuccia, E., Gianelle, V., Močnik, G., Alastuey, A., Olmo, F.J., Alados-Arboledas, L., 2017. Spatial and temporal variability of carbonaceous aerosols: assessing the impact of biomass burning in the urban environment. *Sci. Total Environ.* 578, 613–625. <https://doi.org/10.1016/j.scitotenv.2016.11.007>.
- Tiwari, S., Dumka, U.C., Kaskaoutis, D.G., Ram, K., Panicker, A.S., Srivastava, M.K., Tiwari, Shani, Attri, S.D., Soni, V.K., Pandey, A.K., 2016. Aerosol chemical characterization and role of carbonaceous aerosol on radiative effect over Varanasi in central Indo-Gangetic Plain. *Atmos. Environ.* 125, 437–449. <https://doi.org/10.1016/j.atmosenv.2015.07.031>.
- Tiwari, S., Kaskaoutis, D., Soni, V.K., Dev Attri, S., Singh, A.K., 2018. Aerosol columnar characteristics and their heterogeneous nature over Varanasi, in the central Ganges valley. *Environ. Sci. Pollut. Res.* 25, 24726–24745. <https://doi.org/10.1007/s11356-018-2502-4>.
- Tiwari, S., Kumar, H., Singh, S., Kumar, A., 2023. Current status of aerosol-cloud interactions and their impact over the Northern Indian Ocean: a comprehensive review. *Atmos. Res.* 283, 106555. <https://doi.org/10.1016/j.atmosres.2022.106555>.
- Tiwari, S., Kun, L., Chen, B., 2020. Spatial variability of sedimentary carbon in South Yellow Sea, China: impact of anthropogenic emission and long-range transportation. *Environ. Sci. Pollut. Res.* 27, 23812–23823. <https://doi.org/10.1007/s11356-020-08686-4>.
- Tiwari, S., Pipal, A.S., Srivastava, A.K., Bisht, D.S., Pandithurai, G., 2015. Determination of wood burning and fossil fuel contribution of black carbon at Delhi, India using aerosol light absorption technique. *Environ. Sci. Pollut. Res.* 22, 2846–2855.

- Tiwari, S., Singh, A.K., 2013. Variability of Aerosol parameters derived from ground and satellite measurements over Varanasi located in the Indo-Gangetic Basin. *Aerosol Air Qual. Res.* 13, 627–638. <https://doi.org/10.4209/aaqr.2012.06.0162>.
- Tiwari, S., Srivastava, A.K., Bisht, D.S., Parmita, P., Srivastava, M.K., Attri, S.D., 2013. Diurnal and seasonal variations of black carbon and PM_{2.5} over New Delhi, India: influence of meteorology. *Atmos. Res.* 125, 50–62.
- Vadrevu, K.P., Ellicott, E., Badarinath, K.V.S., Vermote, E., 2011. MODIS derived fire characteristics and aerosol optical depth variations during the agricultural residue burning season, north India. *Environ. Pollut.* 159, 1560–1569. <https://doi.org/10.1016/j.envpol.2011.03.001>.
- Vadrevu, K.P., Ellicott, E., Giglio, L., Badarinath, K.V.S., Vermote, E., Justice, C., Lau, W.K.M., 2012. Vegetation fires in the himalayan region - aerosol load, black carbon emissions and smoke plume heights. *Atmos. Environ.* 47, 241–251. <https://doi.org/10.1016/j.atmosenv.2011.11.009>.
- Vadrevu, Krishna, Lasko, Kristofer, 2015. Fire regimes and potential bioenergy loss from agricultural lands in the indo-gangetic plains. *J. Environ. Manag.* 148, 10–20. <https://doi.org/10.1016/j.jenvman.2013.12.026>.
- Vaishya, A., Raj, S.S., Singh, A., Sivakumar, S., Ojha, N., Sharma, S.K., Ravikrishna, R., Gunthe, S.S., 2023. Black carbon over tropical Indian coast during the COVID-19 lockdown: inconspicuous role of coastal meteorology. *Environ. Sci. Pollut. Res.* 30, 44773–44781. <https://doi.org/10.1007/s11356-023-25370-5>.
- Vaishya, A., Singh, P., Rastogi, S., Babu, S.S., 2016. Aerosol black carbon quantification in the central Indo-Gangetic Plain: seasonal heterogeneity and source apportionment. *Atmos. Res.* 185, 13–21. <https://doi.org/10.1016/j.atmosres.2016.10.001>.
- Venkataraman, C., Habib, G., Eiguren-Fernandez, A., Miguel, A.H., Friedlander, S.K., 2005. Residential biofuels in South Asia: carbonaceous aerosol emissions and climate impacts. *Science* 307, 1454–1456.
- Viana, M., Reche, C., Amato, F., Alastuey, A., Querol, X., Moreno, T., Lucarelli, F., Nava, S., Calzolai, G., Chiari, M., Rico, M., 2013. Evidence of biomass burning aerosols in the Barcelona urban environment during winter time. *Atmos. Environ.* 72, 81–88. <https://doi.org/10.1016/j.atmosenv.2013.02.031>.
- Wang, Q., Huang, R.J., Cao, J., Tie, X., Shen, Z., Zhao, S., Han, Y., Li, G., Li, Z., Ni, H., Zhou, Y., Wang, M., Chen, Y., Su, X., 2016. Contribution of regional transport to the black carbon aerosol during winter haze period in Beijing. *Atmos. Environ.* 132, 11–18. <https://doi.org/10.1016/j.atmosenv.2016.02.031>.
- Weingartner, E., Saathoff, H., Schnaiter, M., Streit, N., Bitnar, B., Baltensperger, U., 2003. Absorption of light by soot particles: determination of the absorption coefficient by means of aethalometers. *J. Aerosol Sci.* 34 (10), 1445–1463.
- Zhang, X., Zhu, Z., Cao, F., Tiwari, S., Chen, B., 2021. Source apportionment of absorption enhancement of black carbon in different environments of China. *Sci. Total Environ.* 755, 142685 <https://doi.org/10.1016/j.scitotenv.2020.142685>.
- Ziola, N., Błaszczyk, B., Klejnowski, K., 2021. Temporal variability of equivalent black carbon components in atmospheric air in southern Poland. *Atmosphere* 12, 119. <https://doi.org/10.3390/atmos12010119>.
- IPCC, 2013: Climate Change 2013: The Physical Science Basis. Contribution of Working Group I to the Fifth Assessment Report of the Intergovernmental Panel on Climate Change. Cambridge University Press, Cambridge, United Kingdom and New York, NY, USA, 1535 pp, doi:10.1017/CBO9781107415324.